

# Soft Crawling Robots: Design, Actuation, and Locomotion

Shoue Chen, Yunteng Cao, Morteza Sarparast, Hongyan Yuan, Lixin Dong, Xiaobo Tan, and Changyong Cao\*

Soft crawling robots have attracted great attention due to their anticipated effective interactions with humans and uncertain environments, as well as their potential capabilities of completing a variety of tasks encompassing search and rescue, infrastructure inspection, surveillance, drug delivery, and human assistance. Herein, a comprehensive survey on recent advances of soft crawling robots categorized by their major actuation mechanisms is provided, including pneumatic/hydraulic pressure, chemical reaction, and soft active material-based actuations, which include dielectric elastomers, shape memory alloys, magnetoactive elastomers, liquid crystalline elastomers, piezoelectric materials, ionic polymer–metal composites, and twisted and coiled polymers. For each type of actuation, the prevalent modes of locomotion adopted in representative robots, the design, working principle and performance of their soft actuators, and the performance of each locomotion approach, as well as the advantages and drawbacks of each design are discussed. This review summarizes the state-of-the-art progresses and the critical knowledge in designing soft crawling robots and offers a guidance and insightful outlook for the future development of soft robots.

high-cost, and unsuitable for interaction with humans as well as intricate environments.<sup>[1–3]</sup> To overcome these challenges, great efforts have been taken to develop soft robots that are primarily made of compliant elastomers and polymers (silicone rubber, dielectric elastomers, liquid-crystalline elastomers and hydrogels, etc.) and possess unique properties such as lightweight, mechanical compliance, infinite degrees of freedom, continuous deformation, low cost, and easy fabrication.<sup>[2–6]</sup> Among these soft robotics, the class of soft crawling robots inspired from biological creatures has attracted increasing attention owing to their anticipated effective interaction with humans and uncertain environments, as well as potential capabilities of completing a variety of tasks, like search and rescue, infrastructure inspection, surveillance, drug delivery, and human assistance.<sup>[2,5]</sup> Various novel actuations and locomotion designs have

## 1. Introduction

Traditional rigid robots can perform faster and more precise position control; however, they are usually bulky, heavy,

been explored to drive soft crawling robots, with some of them even equipped with capabilities of the autonomous motion,<sup>[7]</sup> environment accommodation<sup>[4,8]</sup> and decision making.<sup>[9,10]</sup> For instance, soft crawling robots inspired by octopuses, worms, and jellyfishes have been designed to achieve complex motions with multiple gaits at low cost.<sup>[10,11]</sup> While there have been several excellent review papers on the topic of soft robotics,<sup>[3,4,12,13]</sup> there has not been a review paper that covers recent advances in soft crawling robots in depth. This review paper aims to fill that void.

S. Chen, Y. Cao, M. Sarparast, Prof. C. Cao  
Laboratory for Soft Machines & Electronics  
School of Packaging  
Michigan State University  
East Lansing, MI 48824, USA  
E-mail: ccao@msu.edu

Y. Cao  
Department of Civil and Environmental Engineering  
Massachusetts Institute of Technology  
Cambridge, MA 02139, USA

Prof. H. Yuan  
Department of Mechanics and Aerospace Engineering  
Southern University of Science and Technology  
Shenzhen, Guangdong 518055, China

Prof. X. Tan, Prof. C. Cao  
Departments of Electrical and Computer Engineering, Mechanical Engineering  
Michigan State University  
East Lansing, MI 48824, USA

Prof. L. Dong  
Department of Biomedical Engineering  
City University of Hong Kong  
Kowloon Tong, Hong Kong, China

 The ORCID identification number(s) for the author(s) of this article can be found under <https://doi.org/10.1002/admt.201900837>.

DOI: 10.1002/admt.201900837

The locomotion mode, crawling speed, and working efficiency of soft crawling robots are mainly determined by the soft actuators they employed.<sup>[14]</sup> Generally, the external stimuli drive the actuators to generate the desired strains and/or deformations, and the induced strain and/or deformation will then supply the necessary propulsion for the robots to crawl. Up to now, a few actuation approaches have been successfully employed to drive the soft crawling robots, mainly consisting of pneumatic/hydraulic pressure,<sup>[15]</sup> chemical reaction,<sup>[16,18]</sup> and stimuli responses of soft active materials, such as dielectric elastomers (DEs),<sup>[19]</sup> shape memory alloys (SMAs),<sup>[20]</sup> magnetoactive elastomers (MAEs),<sup>[21]</sup> liquid-crystalline elastomers (LCEs),<sup>[22]</sup> piezoelectric materials (PEMs),<sup>[23]</sup> ionic polymer–metal composites (IPMCs),<sup>[24]</sup> and twisted and coiled polymers (TCPs).<sup>[25]</sup> Despite the inherent drawbacks of these actuation approaches, continuous efforts have been devoted to designing soft crawling robots capable of performing vivid, multigait, effective, and intelligent locomotion. Over the past decade,

thanks to the advances in supportive structures and specific configurations, the overall behaviors of soft actuators have been greatly improved and their application scopes have been largely broadened, enabling the mimicking of locomotion gaits observed in nature to be achieved in soft mobile robots, such as caterpillar-like,<sup>[26]</sup> multigait quadruped,<sup>[27]</sup> worm-like,<sup>[28]</sup> snake-like,<sup>[29]</sup> rolling,<sup>[30]</sup> and jumping modes.<sup>[16]</sup>

In this review, we systematically examine the recent advances in designing soft crawling robots, categorized by major actuation mechanisms, including the pneumatic/hydraulic pressure, chemical reaction, and soft active materials. For each type of actuation, we discuss the prevalent locomotion patterns used in representative crawling robots, the design and working mechanism of their soft actuators, and performance of each locomotion approach, as well as the advantages and drawbacks of the typical prototypes (Table 1). This review summarizes the state-of-the-art progresses and the knowledge in designing soft crawling robots and offers an insightful outlook for the future development of soft robots. Details on the material properties and performance of the soft active materials can be found in some recent excellent reviews in literature.<sup>[13,31,32]</sup>

## 2. Soft Crawling Robots Enabled by Pressure Actuation

### 2.1. Pneumatic Pressure-Based Approach

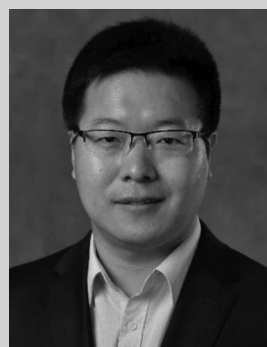
Pneumatic pressure is one of the most popular actuation approaches utilized to drive soft robots. The soft pneumatic pressure-driven actuators are equipped with designed channels that enable the compressed air to inflate the structural walls so as to generate desired deformations (bending, extension, or twisting) for locomotion. One common design is the pneumatic artificial muscle (PAM), which is formed by wrapping the elastomer tubes into a fiber sleeve to generate linear elongation or shrinkage deformation only.<sup>[4]</sup> The main drawbacks of such a design include the potential rupture due to the large pressure/strain needed for effective actuation, and the slow actuation speed due to the relatively low efficiency in pumping/compressing air. To improve the response speed, a pneumatic network (PN) method has been proposed for high speed pressure-driven actuators with the merits of low cost, easy fabrication, and the ability to provide sophisticated motions with simple inputs.<sup>[10,33]</sup> PN-based actuators consist of smaller chamber networks embedded in a deformable soft elastomer body bonded with an unextendible bottom layer (Figure 1A). Bending and rotation of the PN actuator can be easily controlled by tuning the inflation rate, geometry, size, and thickness of the channel walls, as well as chemical and/or structural properties of the materials.<sup>[10,33]</sup> Based on this PN design, Shepherd et al. developed a multigait tetrapod soft robot composed of five PN elastomeric actuators (Figure 1B,C): one located in the spine of the robot to lift off its body from the ground, and the other four on the legs to generate independent bending for motion.<sup>[10]</sup> Through inflating the PN units in rear legs, body, and front legs sequentially, and then deflating them in the same order, this soft robot is able to crawl forward based on anisotropic friction with ground while maintaining a stable



Shou Chen received his B.S. and M.S. degrees in vehicle engineering from Hunan University in 2014 and 2018, respectively. He is currently working toward his Ph.D. degree at the Laboratory for Soft Machines and Electronics under the supervision of Prof. Changyong Cao at Michigan State University. His research interests include smart materials and structures, soft robotics and soft machines, and triboelectric nanogenerators.



Xiaobo Tan is an MSU foundation professor in electrical and computer engineering at Michigan State University. He received his B.S. and M.S. degrees in automatic control from Tsinghua University, Beijing, China, in 1995 and 1998, respectively, and his Ph.D. in electrical and computer engineering from the University of Maryland in 2002. His research interests include electroactive polymer sensors and actuators, modeling and control of systems with hysteresis, soft robotics, and bioinspired underwater robots with application to environmental sensing. He is also a fellow of IEEE and ASME.



Changyong Cao is an assistant professor in the School of Packaging, and Departments of Mechanical Engineering and Electrical & Computer Engineering (by courtesy) at Michigan State University, where he is directing the Laboratory for Soft Machines and Electronics. He received his Ph.D. degree in mechanical engineering and materials science from the Australian National University in 2014, and then worked as a postdoctoral research associate at Duke University. His research interests include the mechanics and physics of soft materials, soft robotics, smart materials, printed electronics, flexible/stretchable electronics, smart packaging system, as well as the 3D/4D printing of advanced functional materials.

**Table 1.** Summary of the representative soft crawling robots reviewed.

Actuation	Robot design	Locomotion mechanism	Pros and cons	Speed [mm s <sup>-1</sup> ]	Weight [g]	Operation situation	Refs.
Pneumatic/ hydraulic pressure	Tripedal/quadruped/ hexapod	Gravity center shift induced by bending of legs	<ul style="list-style-type: none"> <li>• PNs functioning as soft body and actuators simultaneously</li> <li>• Simple locomotion gait</li> </ul>	25.6	–	7 psi atmospheric pressure	[10]
			<ul style="list-style-type: none"> <li>• Flexion and extension of legs via a double channel design</li> <li>• Low actuating force in legs</li> </ul>	–	–	Air pressure ranging from 0 to 5 bars	[46]
			<ul style="list-style-type: none"> <li>• All components printed in a single step (ready-to-use)</li> <li>• Printed hydraulics enabling complex robotic designs</li> </ul>	17.5	690	Geared DC motor turns the crankshaft at 30 rpm	[15]
	Snake/ caterpillar-like	Actuation of adjacent chambers in cVAMs to rotate the legs	<ul style="list-style-type: none"> <li>• More locomotion gaits with increased DOFs of cVAMs</li> <li>• Bulky input components</li> </ul>	5	–	Vacuum from –5 to –90 kPa	[42]
		Slithering by bidirectional bending and double-helical thread frictional skin	<ul style="list-style-type: none"> <li>• Realizing shape space design that enables optimal gaits</li> <li>• Arbitrary actuators linked effectively using magnets</li> </ul>	1.96	–	Air pressure from 0 to 24 kPa	[29]
Dielectric elastomer (DE)	Quadruped/ hexapod	Elongation/shrinkage of body with kirigami-enabled anisotropic friction	<ul style="list-style-type: none"> <li>• Kirigami-enabled anisotropic frictional skin for crawling</li> <li>• Untethered design with improved adaptability</li> </ul>	8.75	>65	Air volume is cyclically varied between 0 and 12 mL	[37]
		Omnidirectional and rotary motions by the contraction of chambers in different modules	<ul style="list-style-type: none"> <li>• Convenient modular and reconfigured design for various tasks</li> <li>• Bulky input devices and complex control</li> </ul>	5.14	50–90 (each module)	Pressure of 5 kPa and vacuum degree of 10 kPa	[44]
		Curvature change of legs and anchor-pulling effect	<ul style="list-style-type: none"> <li>• Suitable for modular design</li> <li>• Limited DOFs of legs</li> </ul>	5.75	–	Applied electric field of 50 V μm <sup>-1</sup>	[27]
		Rectilinear movements of legs by contracting of stacked DEAs	<ul style="list-style-type: none"> <li>• Large deformation induced by stacked DEAs</li> <li>• Bulky transmission parts</li> </ul>	–	450	Sinusoidal voltage 3.5 kV, 1–10 Hz	[56]
	Close-looped	Lifting and swinging bidirectionally of legs by antagonistic DEAs		<ul style="list-style-type: none"> <li>• Convenient for robotics modular design</li> <li>• Promising DEA design for more DOFs</li> </ul>	4	80	Square voltage of 3.5 kV, 0.5 Hz
<ul style="list-style-type: none"> <li>• Simplified and light structure suitable for modular design</li> <li>• Low adaptability</li> </ul>				52	20	Square voltage of 3.5 kV, 1 Hz	[59]
Indirect rolling through wheels powered by antagonistic DEAs			<ul style="list-style-type: none"> <li>• Improved performance of foldable antagonistic DEA</li> <li>• Bulky supportive components</li> </ul>	42	45	Cyclic triangle voltage 7.4 kV (T = 2 s, ramping rate 15 kV s <sup>-1</sup> )	[62]
			<ul style="list-style-type: none"> <li>• Large speed–mass ratio</li> <li>• Continuous motion but flat ground required</li> </ul>	36.27	0.88	Alternating high and low voltages (3.2 kV, 0 V), duration time ≈ 370 ms	[30]
			<ul style="list-style-type: none"> <li>• Omnidirectional motion realized by DEMES and EAAs</li> <li>• Limited deformation range of the robot's body</li> </ul>	1.95	1.10	Square-wave voltage of 3 kV, 1 Hz	[65]
Caterpillar/ inchworm-like	Curvature change or expansion/shrinkage of robot's body, and anisotropic friction		<ul style="list-style-type: none"> <li>• Simplified and light structure suitable for modular design</li> <li>• Low adaptability</li> </ul>	–	6.3	–	[66]
			<ul style="list-style-type: none"> <li>• Untethered and capable of turning via EAAs</li> <li>• Bulky hard components</li> </ul>	4.16	3.5	Step voltage of 3 kV on EAAs and ramping voltage to 6 kV on DEA	[28]

**Table 1.** Continued.

Actuation	Robot design	Locomotion mechanism	Pros and cons	Speed [mm s <sup>-1</sup> ]	Weight [g]	Operation situation	Refs.
			<ul style="list-style-type: none"> <li>Completely soft by combining DEOs and DESs</li> <li>Limited locomotion space</li> </ul>	–	–	–	[26,69]
Shape memory alloy (SMA)	Caterpillar/ inchworm-like	Curvature change of robot's body and anchor-pulling effect	<ul style="list-style-type: none"> <li>Effective rolling motion</li> <li>Ballistic rolling ending with an unpredictable tumble</li> </ul>	200	6.2	400 mA (five 0.125 s DC pulses at 2 Hz)	[20]
		Curvature change or relative movement of body parts as well as anisotropic friction	<ul style="list-style-type: none"> <li>Deformation wave realized by overlapped SMAs</li> <li>Switchable friction design</li> </ul>	2.2	–	Power supply of 7.5 V to heat SMAs, phase gap 0.1–10 s	[75]
	Starfish-like	Gravity center shifting via tentacle bending	<ul style="list-style-type: none"> <li>Improved LIP SMA actuator</li> <li>Crawl bidirectionally and steer</li> </ul>	9	1.2	0.35 A current for heating, 1 Hz	[78]
	Turtle-like	Bending and twisting of SSCs in various levels	<ul style="list-style-type: none"> <li>High adaptability (climbing, steering, and navigating)</li> <li>No good underwater motion</li> </ul>	1.1	75 (6-rayed)	–	[76]
Magnetoactive material (MAE)	Caterpillar/ inchworm-like	Rotation and deflection in different degrees induced by designed magnetic fields	<ul style="list-style-type: none"> <li>Large coupled bending and twisting deformation</li> <li>No good terrestrial motion</li> </ul>	22.5	82.5	900 mA (in air), 1300 mA (in water)	[77]
		Rolling generated by a rotating magnetic field	<ul style="list-style-type: none"> <li>Strong carrying and obstacle-crossing capacities</li> <li>Survive in harsh environment</li> </ul>	0.5	0.04	Max magnetic torque to foot ≈0.4 nN m, 1 Hz	[21]
	Hexapedal		<ul style="list-style-type: none"> <li>Transit reversibly between various liquid and solid terrains</li> <li>Small-scale and flexible</li> </ul>	–	–	Programmed magnetic fields	[80]
			<ul style="list-style-type: none"> <li>Excellent shape changing ability</li> <li>Deliver objects with arbitrary shape on demand</li> </ul>	–	≈170	Programmed magnetic fields	[83]
Liquid crystalline elastomer (LCE)	Caterpillar/ inchworm-like	Curvature change of robot's body and anchor-pulling effect	<ul style="list-style-type: none"> <li>Large and rapid-responsive motions via photoirradiation</li> <li>Simple locomotion gait</li> </ul>	–	–	UV (366 nm, 240 mW cm <sup>-2</sup> ) and visible light (>540 nm, 120 mW cm <sup>-2</sup> )	[85]
			<ul style="list-style-type: none"> <li>Sense the environment and response in an adaptive fashion for locomotion</li> <li>Lightweight but inefficient gait</li> </ul>	0.03	0.29	0.069 W power to heat for 15 s in each step	[22]
		Local contraction of robot's body associated with curly bending (wave-like pattern)	<ul style="list-style-type: none"> <li>Different gaits realized by varying lighting conditions</li> <li>Constrained motion due to requirement for laser beam scan</li> </ul>	0.24	<0.03	Continuous wave green laser beam of 2.5 W, 0.4 Hz	[87]
Piezoelectric material (PEM)	Inchworm-like	Curvature change of robot's body and the anchor-pulling effect	<ul style="list-style-type: none"> <li>Large curvature changes generated by small voltages</li> <li>Simple motion and low adaptability</li> </ul>	1.9	–	Sinusoidal voltage 200 V, 16 Hz	[23]
Ionic polymer–metal composite (IPMC)	Caterpillar-like	Expansion and contraction of body units along with gripping/opening of legs	<ul style="list-style-type: none"> <li>Modular design of body and leg units, easy for assembly</li> <li>Various possible gaits</li> <li>Easy fabrication of IPMCs via 3D printing</li> </ul>	0.157	–	Voltage amplitude of 2.5 V with a frequency of $\pi/2$ rad s <sup>-1</sup>	[90]
Twisted and coiled polymer (TCP)	Caterpillar/ inchworm-like	Curvature change of robot's body and the anchor-pulling effect	<ul style="list-style-type: none"> <li>Simple design with low cost</li> <li>Low efficiency due to long cooling time</li> </ul>	0.245	–	Power of 0.16 W cm <sup>-1</sup> , 5 s for heating/cooling	[92]
			<ul style="list-style-type: none"> <li>Simple design with low cost</li> <li>Low directional stability</li> </ul>	1.2	9	Temperature from 60 to 100 °C with a period of 5 s	[93]

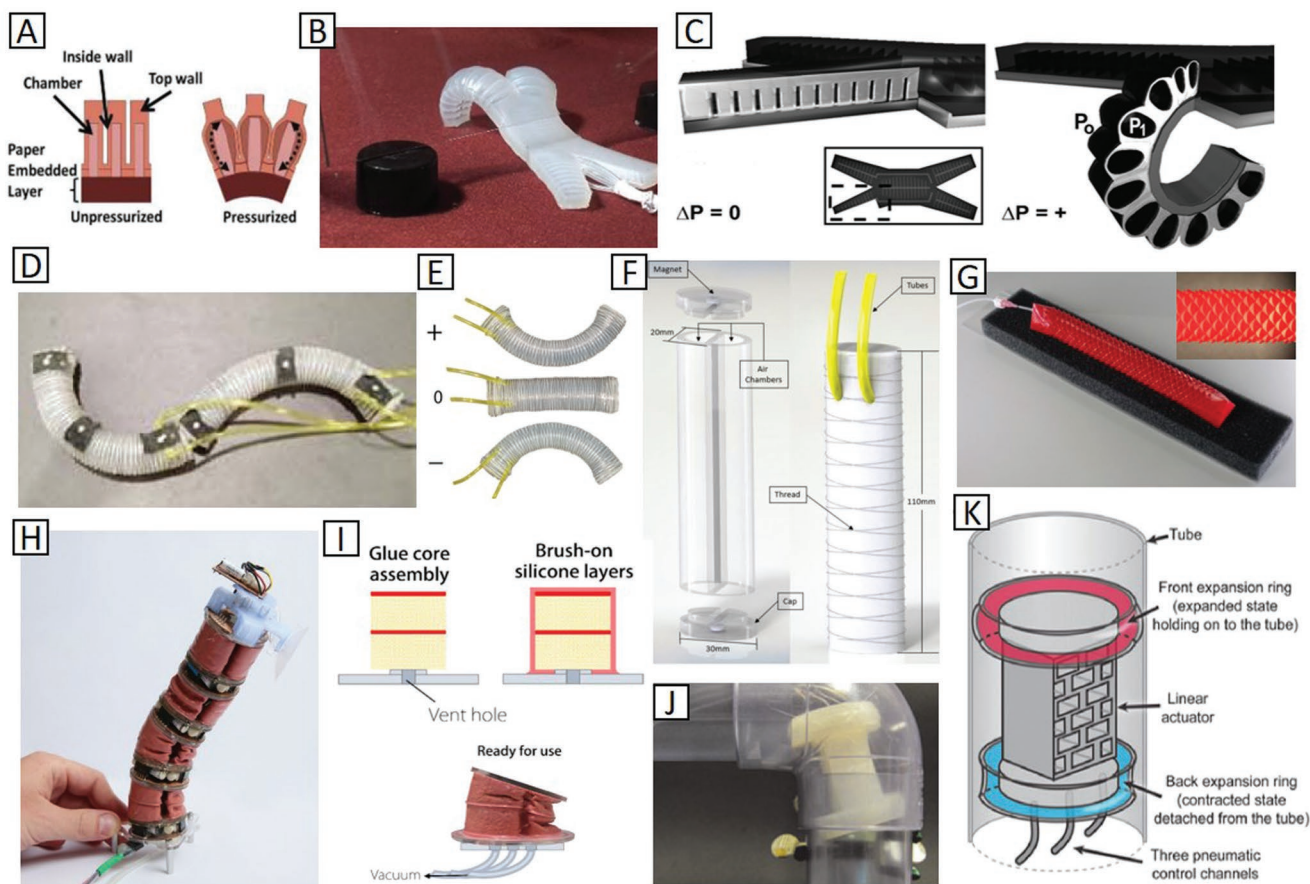


**Figure 1.** Soft crawling robots actuated by pneumatic pressure. A) Shape-change principle of a PN actuator. Reproduced with permission.<sup>[33]</sup> Copyright 2014, Wiley-VCH. B) A multigaft soft robot, and C) the cross-section of the soft PN channels under two different pressure states. Reproduced with permission.<sup>[10]</sup> Copyright 2011, National Academy of Science. D) A soft snake-like robot, E) mechanical design for undulatory locomotion, and F) depiction of actuator assembly in its design. Reproduced with permission.<sup>[29]</sup> Copyright 2017, IEEE. G) A kirigami-skinned crawler. Reproduced with permission.<sup>[37]</sup> Copyright 2018, American Association for the Advancement of Science. H) A continuum robot comprising four V-SPA modules, and I) structure of the V-SPA. Reproduced with permission.<sup>[39]</sup> Copyright 2017, American Association for the Advancement of Science. J) A soft tube-climbing robot, and K) schematic view of it containing a VAMP and two pressure-actuated rings. Reproduced with permission.<sup>[40]</sup> Copyright 2018, Mary Ann Liebert Inc.

state in motion.<sup>[34]</sup> Different locomotion gaits can be achieved by changing its inflation and deflation sequences and the typical speed of the soft robot made of Ecoflex 00-50 can reach  $\approx 1.53 \text{ m min}^{-1}$ , actuated by an air pressure of 7 psi.

Control strategies remain a nascent area of research for soft robotics due to the intrinsic nonlinear behaviors of soft structures. To address this issue, Branyan et al. proposed a soft snake robot that utilized the high-curvature continuum bending of pneumatic actuators to generate slithering gaits (Figure 1D).<sup>[29]</sup> The robot has equipped a pair of parallel chambers along the tube to achieve bidirectional bending, and a double-helical thread wrapping pattern to disrupt the gait pattern by preventing twisting upon inflation. The elliptical cross-section prevents the robot from rolling upon actuation, leading to a much more decent locomotion with an average speed of  $11.7 \text{ cm min}^{-1}$  (Figure 1E,F). Similarly, soft snake-like robots are also designed based on the friction-assisted locomotion<sup>[35]</sup> and engineered surfaces with programmable tribological behaviors.<sup>[36]</sup> Recently, Rafsanjani et al. reported a soft crawler composed of a soft prism-shaped pneumatic actuator wrapped by a kirigami skin made of a thin plastic sheet (Figure 1G).<sup>[37]</sup>

The crawling of the robots enabled by the anisotropic friction generated from the kirigami skin, is attributed to the buckling triggered by the elongation of the fiber-reinforcement actuator upon inflation. The efficiency of the kirigami-skinned crawler can be further improved by optimizing the cut geometry and actuation protocol to balance the frictional properties and the stretchability of its skin.<sup>[38]</sup> With lightweight on-board control, sensing, actuation, and power source (45 g), this soft robot can be fully untethered. By alternatively inflating and deflating the actuator, an optimal locomotion can be obtained through a design with trapezoidal cuts.

Besides the positive pneumatic pressure, the negative pneumatic pressure (vacuum) is also employed to drive soft robots. For example, Robertson and Paik developed a vacuum-powered soft pneumatic actuator (V-SPA) and built versatile robots with multiple degrees of freedom (DOF) (Figure 1H).<sup>[39]</sup> A V-SPA module contains three evenly spaced actuation channels in a cylindrical configuration, and each channel is connected to a centralized vacuum supply. The lightweight actuator has a 2D polyurethane foam core and rigid paper dividers to prevent the buckling on the upper surface and intervals. Also, a silicone

rubber layer is coated on the external surfaces of the actuator to seal pores in order to prevent air leakage (Figure 1I). The angular deflection is generated once the activated actuators between the plates contract, which can be employed to make robot crawl forward. In another study, Verma et al. combined the pneumatic actuation and the vacuum actuation to drive a soft robot capable of climbing in a tube (Figure 1J).<sup>[40]</sup> The body of the climbing robot is a vacuum-actuated muscle-inspired pneumatic structure (VAMP) actuator with a pair of ring-shaped pneumatic actuators mounted on its two ends.<sup>[41]</sup> The VAMP is structured with interconnected elastomeric beams to support one another in the chamber and its outer surface is sealed by a thin elastomeric membrane to prevent air leakage (Figure 1K). In one climb cycle, the front ring-like actuator first expands to hold against the tube wall, but the back ring-like actuator contracts to detach from the tube. Then, a vacuum pressure is applied to the void chambers of the body to produce a linear motion, induced by the buckling of the horizontal beams in the body. Next, the back ring-like actuator expands against the tube wall again, while the front ring-like actuator contracts to release the robot from the tube. Once the body actuator extends to its original length upon vacuum release, the front ring moves forward to complete one step. Through programmed controlling of the expansion and

contraction of the two rings and the VAMP body, the robot can climb along a tube quickly.<sup>[41]</sup>

In addition to the crawling gaits, advanced locomotion patterns (e.g., walking, rotating, and hopping) provide new alternative strategies for designing soft robots. For example, adding rigid frames or coupling with multiple modules imparts reconfigurable and omnidirectional features to the soft actuators. As shown in Figure 2A, a soft quadrupedal robot is designed to mimic a reptilian gait, i.e., simultaneously moving diagonal limbs, equipped with four cyclical vacuum-actuated machines (cVAMs).<sup>[42]</sup> The cVAM has four pneumatic chambers which can be inflated by pressurization or deflated by vacuum independently, arranged in a ring-shaped configuration with a rigid rod positioned in the center. Through sequential actuation of the adjacent chambers can rotate the tip of the central rod in a cyclic manner, which can be further utilized to locomote the robot (Figure 2B,C). The prototype of the robot can crawl at a speed of  $\approx 0.5 \text{ cm s}^{-1}$  when the vacuum state changes every 0.1 s.

Reconfigurable and omnidirectional soft robots have been developed for applications in unstructured environments.<sup>[43]</sup> For instance, Zou et al. developed a pneumatic-driven, modular, and reconfigurable soft crawling robot, capable of both translation and rotation motions (Figure 2D).<sup>[44]</sup> Each module

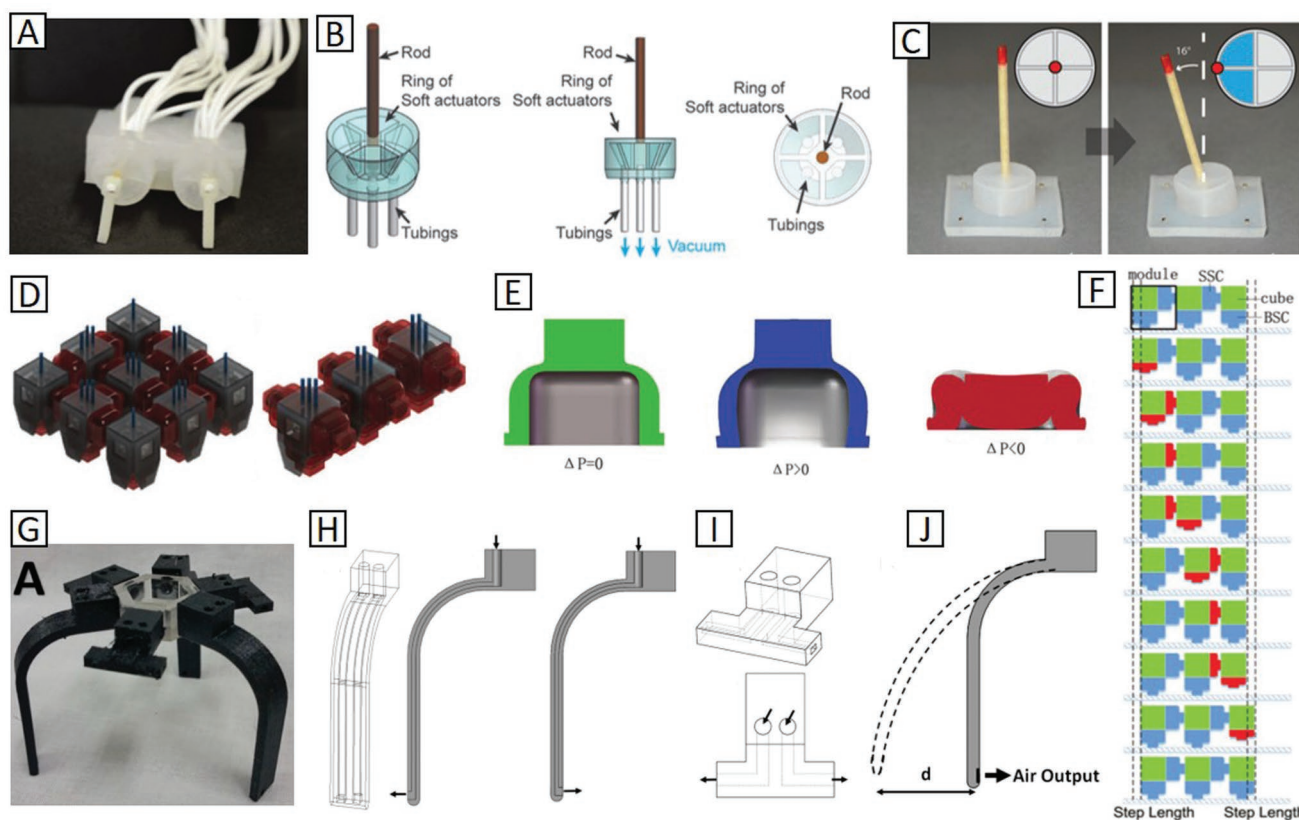


**Figure 2.** Soft crawling robots in walking modes actuated by pneumatic pressure. A) A four-legged soft robot, B) structural design of the cVAM, and C) its actuation via applying a negative pressure of  $-90 \text{ kPa}$ . Reproduced with permission.<sup>[42]</sup> Copyright 2017, Mary Ann Liebert Inc. D) An omnidirectional soft robot consisting of nine (left) and three (right) modules, E) deformation of the soft cylinder under various conditions, and F) mechanism of crawling gait including contracted (red), pressurized (blue), and structure parts (green). Reproduced with permission.<sup>[44]</sup> Copyright 2018, Mary Ann Liebert Inc. G) A tripod soft robot actuated based on the air propulsion actuator, H) air propelled limb and I) thrusts (arrows show the direction of air flow), and J) the horizontal displacement of the limb during bending. Reproduced with permission.<sup>[46]</sup> Copyright 2018, MDPI.

of the robot contains two different parts: the cube serving as the structural component and the soft pneumatic cylinder-shaped actuator fixed to the sides (named S-SC) or bottom of the cubes (named B-SC). The S-SCs and B-SCs have the same shape and are able to be actuated by both positive and negative pressures. Figure 2E shows the deformations of the soft cylinder under different pressures. As shown in Figure 2F, a  $1 \times 3$  module array is combined to mimic the crawling gait of caterpillars. The crawling motion can be generated by actuating the modules from back to front, i.e., both B-SCs and S-SCs are first pressurized; the B-SC in the rear is then contracted by a negative pressure to detach from the ground; next, the adjacent S-SC is contracted to push the module forward; and finally, the B-SC is pressurized again to touch the ground. Furthermore, based on modular design, a  $3 \times 3$  array can obtain three DOFs to produce propagating waves in two orthogonal directions for a translational movement, and two waves in opposite directions for clockwise/counterclockwise rotation. In this case, the traveling wave is propagated along the backward and forward directions or the left and right directions. This enhanced robot can reach an arbitrary point on a plane in any angle, manifesting the property of omnidirectionality.

Unlike inflated and deflated chambers, the use of air propulsion to drive locomotion in soft robots is almost untapped, even though this technology has been around for a long time.<sup>[45]</sup> Air propulsion provides larger motion degrees in limb actuators than those of pneumatic actuators based on expandable air channels, which are limited by air pressure input, cyclic fatigue, and minimum size. For instance, Chua and Yeow designed a tripedal, air-driven soft robot fabricated by 3D printing, which is able to perform biomimetic motions such as crawling, grasping, kicking, and picking of objects (Figure 2G).<sup>[46]</sup> The soft robot has three flexible limbs and three lateral thrusters. The limbs are designed to mimic the simple flexion and extension, which require two separate air channels to be incorporated side by side within each limb (Figure 2H). The three lateral thrusters enable the robot to rotate quickly and to change its moving direction. The thrusters also have paired but oppositely aligned air channels (Figure 2I). The flexion and extension of the limbs are attained through channeling the pressurized airflow into either of the two top inlets. Each gait cycle starts off with the extension of its frontal limb, followed by the flexion of its right rear limb and finally the flexion of the left rear limb. To achieve hopping, higher air pressure (>4 bar) is used to generate a higher acceleration through the back-facing outlet of the frontal limb (Figure 2J).

## 2.2. Hydraulic Pressure-Based Approach

Hydraulic actuators can be considered as ancestors of pneumatic actuators. The main difference between these two approaches is the higher viscosity and lower compressibility of fluid used in hydraulic actuators.<sup>[47]</sup> Theoretically, most of the soft robots presented in Section 2.1 driven by pneumatic pressure can also be actuated hydraulically. Figure 3A shows a soft robot actuated hydraulically, which is fabricated based on multimaterial 3D printing that can print both rigid and liquid components simultaneously.<sup>[15]</sup> This hexapod robot can mimic

a tripod gait with six rotational DOFs imparted by the bellow structure connected to each leg. A fluidic channel runs through the body and connects the driving bellows to the driven ones. When the crankshaft linked to a set of bellows pumps is turned on, the fluid is pumped out and delivered to each soft actuator connected with a leg, leading to friction-based locomotion. The configuration of the six legs (three legs inclined toward rear and the other three along  $90^\circ$  out of phase) makes both forward and backward motions feasible without any additional DOF of each leg (Figure 3B,C). The as-developed soft robot attains a speed of 0.125 body-length per second ( $1.75 \text{ cm s}^{-1}$ ) at the crankshaft speed of 30 rpm.

## 2.3. Chemical Reaction-Based Approach

Direct chemical reactions to generate gas and/or heat, such as monopropellant decomposition, combustion, and hypergolic reactions, have been proposed as a promising propulsion approach for soft robots due to their potential to replace the built-in batteries or tethered external power source.<sup>[18,48]</sup> Wehner et al. developed an “Octobot” robot powered by monopropellant fuel and controlled by a microfluidic logic (Figure 3D).<sup>[18]</sup> Multimaterial 3D printing technology is used to pattern the networks for pneumatic actuators, on-board fuel reservoirs, and catalytic reaction chambers inside the robotic body.<sup>[49]</sup> Adopting pressure-activated valves and switches, the eight arms of the robot can be evenly separated into two alternating groups (red and blue colored in Figure 3E). The flexible microfluidic circuit directs the flow of a liquid fuel, i.e., 50% hydrogen peroxide solution, to the reaction chamber, rapidly producing a large volume of oxygen when exposed to platinum catalyst. The oxygen is pressurized, concurrently flowing downstream into the actuators (Figure 3F).<sup>[17]</sup> This work provides a new approach for designing untethered soft robots driven by chemical reactions.

Combustion usually needs a fuel (e.g., methane or butane) and an oxidant (e.g., oxygen) in the presence of flame or spark. Bartlett et al. fabricated a combustion-driven jumping soft robot by utilizing multimaterial 3D printing.<sup>[16]</sup> This soft jumper comprises a rigid core module containing control and power components protected by a semisoft shield, an explosive actuator, and three pneumatic legs (Figure 3G). Oxygen and butane are delivered into the combustion chamber alternately, and then the mixture is ignited for combustion, resulting in ballooning out of the bottom hemispheroid to push against the ground and to propel the robot into the air (Figure 3H,I). By utilizing 40 mL butane and 120 mL oxygen, the robot is able to jump as high as 0.76 m vertically and move 0.15 m laterally along a specific direction. In addition, this robot allows for 21 untethered jumps and 89 tethered jumps with no significant damage on the body. It is noted that although chemical reaction is utilized to generate gas to propel the motion of the soft robots in the presented designs, it is significantly different from the aforementioned pressure-based actuation approaches, which usually need extra pumps with tethered tubes for supplying the pressure. The unique chemical reaction-based propulsion strategy enables soft robots to be untethered and self-powered, which is a unique advantage in developing autonomous crawling robots

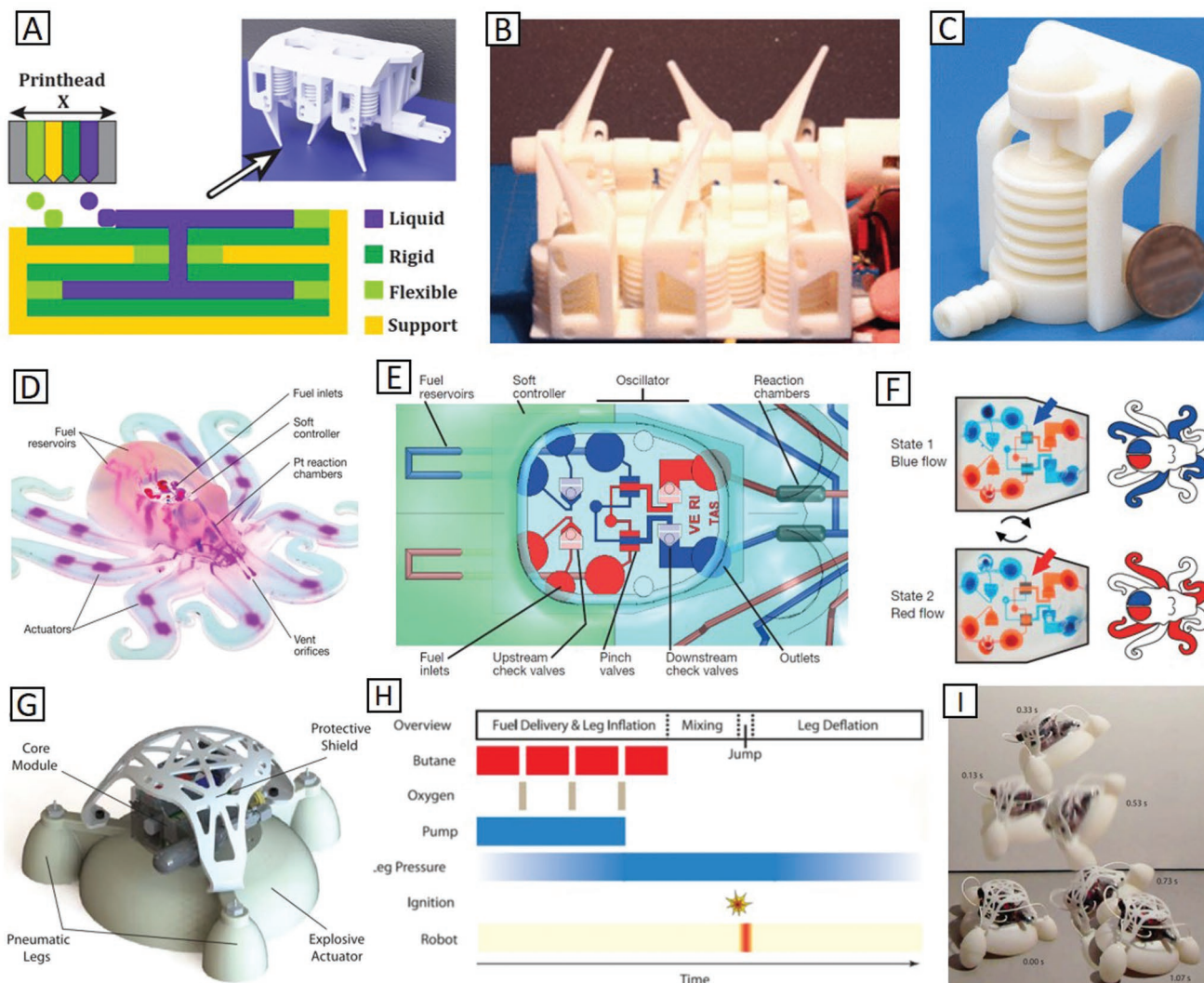


**Figure 3.** Soft crawling robots driven by hydraulic pressure and chemical reaction. A) A hexapod robot involving one-step fabrication by inkjet that simultaneously deposits solid and liquid layers within a printed assembly, B) position of its legs that incline their major axis  $60^\circ$  above the floor, and C) the bellows structure connected with each leg. Reproduced with permission.<sup>[15]</sup> Copyright 2018, IEEE. D) A fully soft and self-contained Octobot actuated by the monopropellant decomposition, E) its system of check valves and switch valves within the soft controller (discrete sides are depicted in red and blue for clarity), and F) oscillator of the soft controller causes the Octobot robot to alternate between actuation states. Reproduced with permission.<sup>[18]</sup> Copyright 2018, Springer Nature Group (SNG). G) A 3D-printed, functionally graded soft robot driven by combustion, H) ignition sequence involving fuel delivery, mixing, and sparking, and I) its position at various time steps during a directional jump. Reproduced with permission.<sup>[16]</sup> Copyright 2018, American Association for the Advancement of Science.

and is expected to attract more attention in the future for developing next-generation soft mobile robots.

### 3. Soft Crawling Robots Enabled by Soft Active Materials

#### 3.1. Dielectric Elastomers

DEs have been widely adopted in fabricating soft actuators due to their large actuation strain, high compliance, and high energy density.<sup>[50]</sup> DEs are able to respond to electrical stimuli to generate large deformations and/or shape changes.<sup>[51]</sup> A typical DE actuator (DEA) is made of a thin DE film with compliant

electrodes coated on both surfaces, forming a parallel plate capacitor. When a voltage is applied to the compliant electrodes, opposite charges will be induced on both sides of the film, generating the Maxwell stress to compress the film to shrink along its thickness direction while to expand in-plane. Based on this principle, various types of DEA have been proposed, including stack, bimorph and unimorph, diaphragm, bulged membrane, and spring-roll designs.<sup>[52]</sup> Since the invention of the first DEA-based walking robot (FLEX),<sup>[53]</sup> the focus of the DAE-based crawling robots has been placed on how to improve the moving speed and increase the DOFs for locomotion.<sup>[54,55]</sup> For example, Nguyen et al. proposed a quadruped walking robot actuated by multistacked DEAs where multiple layers of DE films are stacked and connected in parallel (Figure 4A,B).<sup>[56]</sup> To avoid

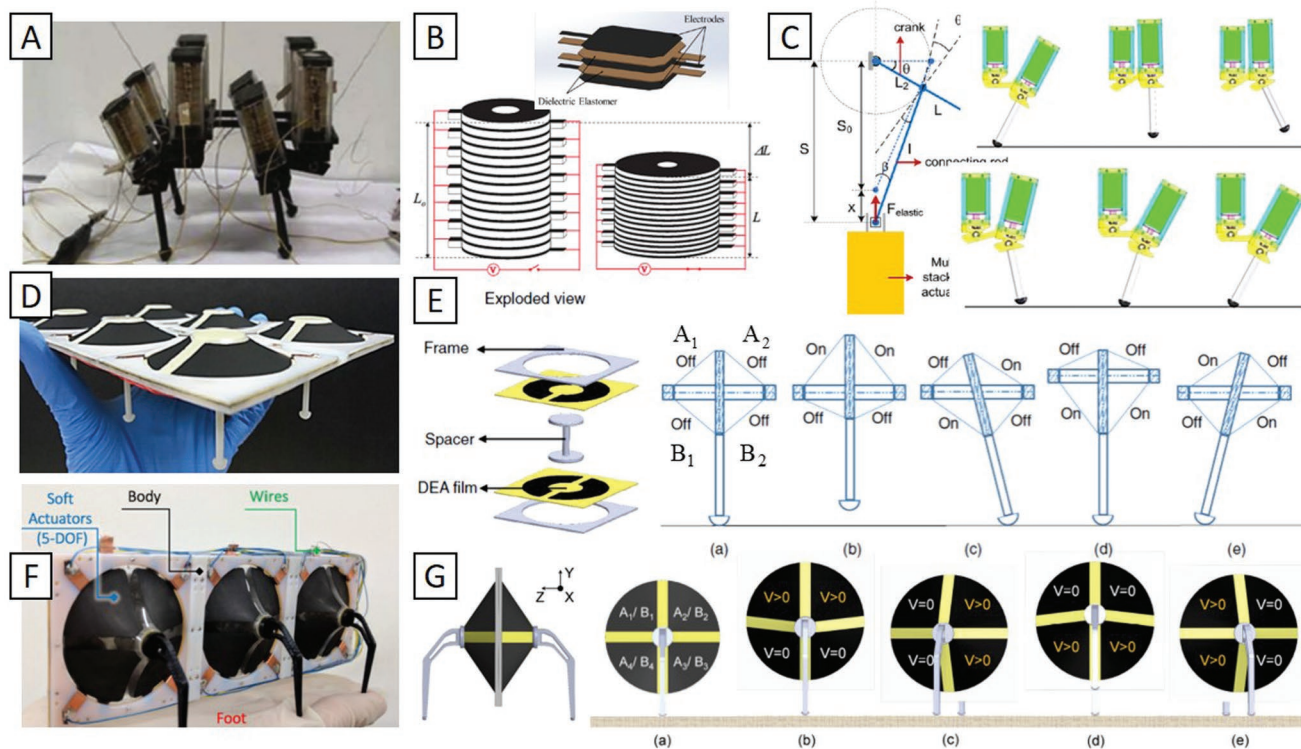


**Figure 4.** Soft crawling robots in walking modes actuated by dielectric elastomers. A) A biomimetic quadruped robot based on multistacked DEAs, B) operating principle of the multistacked DEA, and C) operating postures of the quadruped robot's leg: the swing phase (upper ones) and stand phase (lower ones) with the mechanism of the slider crank. Reproduced with permission.<sup>[56]</sup> Copyright 2014, IOP. D) The first generation Sungkyunkwan hexapod robot, S-Hex I, and E) its leg design and postures in a walking cycle: a) passive state, b) lifting upward, c) swinging forward, d) pushing downward, and e) swinging backward. Reproduced with permission.<sup>[58]</sup> Copyright 2015, IEEE. F) The second generation Sungkyunkwan hexapod robot, S-Hex II, and G) its leg design and postures in a walking cycle, including a) passive state, b) pushing downward, c) swinging backward, d) lifting upward, and e) swinging forward. Reproduced with permission.<sup>[59]</sup> Copyright 2017, IEEE.

the nonuniform deformations due to the free edge of folded trapezoidal and rectangular actuators, the new multistacked DEA is developed by sandwiching two DE films with three electrodes (Figure 4B).<sup>[57]</sup> The proposed multistacked DEA weights 9.68 g with  $\approx 58$  layers (23 mm) and is able to produce a 10% compressive strain under a sinusoidal voltage of 5 kV with a frequency of 0.5 Hz when measured with a 50 g mass on the top of it. In their design, two DEAs are used in each leg and a slider crank mechanism is used to convert the linear motion of multistacked actuators to swing and stance phases of the leg of the robot (Figure 4C). The vertical movement of the piston induced by the applied voltage would be transferred to the crank through a connecting rod and generate rotation. However, this design suffers from the leg's low DOF, increased mass, and complex mechanical structures, which constrain its versatility and efficiency.

A scalable hexapod robot (S-Hex I) using six multi-DOF DEAs was proposed in another study by Nguyen et al. (Figure 4D).<sup>[58]</sup> Inspired by a cockroach, they embed multi-DOF DEAs into the body of a robot with stick-like legs (Figure 4E). The multi-DOF DEA consists of two DE films bonded to the rigid frames and assembled through a spacer, which is sandwiched at the center and acts as a pretensioner. When no voltage is applied, the robot maintains its original configuration due to the force balance resulting from its axial symmetry. When one active region (coated

with electrodes) of each DE film is stimulated, it expands and the tension inside declines, resulting in the initial balance breaking and the motion of the pretensioner toward the actuated regions due to a higher tension in the opposite region.<sup>[58]</sup> The stance and swing phases of the robot leg, which is essential to walking motions, can be generated by alternatively actuating the active elements on the DEA (Figure 4E). This antagonistic multi-DOF actuator exhibits a better performance than the folded DEAs owing to its simpler configuration and a larger DOF, yet still suffers from relatively high weight, large size, sophisticated assembling process, and relatively low speed ( $4 \text{ mm s}^{-1}$  for the forward and backward motions of the robot, under a square voltage of 3.5 kV and a frequency of 0.5 Hz). Later on, Nguyen et al. developed a new robot, S-Hex II, with a smaller size and more than 12 times the speed ( $52 \text{ mm s}^{-1}$ ) compared to that of S-Hex I (Figure 4F).<sup>[59]</sup> This improvement is attributed to the enhanced 5-DOF actuator (Figure 4G),<sup>[60]</sup> where the electrode coated on each DE film is divided into four regions, improving the total DOF into 5. Different from the fabrication of S-Hex I, the initial synthetic elastomer (SE) used is modified to improve its tearing strength for allowing a larger prestrain to be applied onto the DE membrane to attain a higher electromechanical strain. It is demonstrated that the improved 5-DOF DE actuator with a weight of 4 g can generate a higher stroke (2.58 mm), larger rotation ( $16.4^\circ$ ), and higher output force (0.124 N) and torque (1.08 N mm).

Mobile robots fabricated by DEAs usually contain undesirable bulky structures to support their motions. To reduce the sizes of robots but increase their agility, other locomotion patterns (e.g., rolling) have been explored to simplify the structural design. Some soft robots capable of rolling exhibit higher speeds by integrating stiffen components, but may suffer poor adaptability to the environment.<sup>[61]</sup> As illustrated in **Figure 5A**, Sun et al. developed a crawling robot with rolling wheels using foldable DEAs.<sup>[62]</sup> This robot has two pairs of rigid wheels, two enhanced foldable DEAs, and two cantilever structures to connect the DEA and the axles of the wheels. The enhanced foldable DEA is fabricated with rigid bars to keep the prestretched DE film in a specific direction (pure shear deformation).<sup>[63]</sup> In order to generate a unidirectional locomotion, two gears are fixed coaxially to the wheels, and two patches are attached on the frame to engage gear teeth (Figure 5B). Four prestretched DE films are connected through a rigid spacer, while a cantilevered hinge is symmetrically placed across the spacer and the opposite DE membranes can lead to an antagonistic actuation mode (Figure 5C). Without voltage, the opposite DE films attain an equilibrium state with a folding angle due to different prestretch strains. Once a voltage is applied, the actuator will bend downward, breaking the previous equilibrium of the DEAs to generate a larger folding angle along with deformations of the frame. A 25° folding angle can be achieved under an applied voltage of 7.3 kV. The maximum rolling speed of this robot is

$\approx 42 \text{ mm s}^{-1}$  by applying a cyclic triangle voltage with an amplitude of 7.4 V (ramping rate  $15 \text{ kV s}^{-1}$  and  $T = 2 \text{ s}$ ).

To improve the environmental adaptabilities, innovative structures without rigid parts (e.g., gears, linkages, wheels) have also been developed for soft rolling robots. As shown in **Figure 5D**, a rolling soft robot (RSR) was built by connecting the multisegmental dielectric elastomer minimum energy structures (DEMES) to form a ring-like configuration.<sup>[30]</sup> This rolling robot stays in an equilibrium shape when the prestrain in DEMES is released, where the resilience of the frame is balanced by the contraction force from the DE films. As a high voltage is applied to either active area, the induced Maxwell stress bends the DEMES correspondingly and change its ring-like shape (Figure 5E), resulting in a rotational momentum due to the deviation of the gravity center of the robot.<sup>[64]</sup> When the DEs in the opposite direction are actuated by an applied voltage of 3.2 kV, the RSR can immediately transfer its shape from a circle to an ellipse within 50 ms. This high response frequency and the lightweight feature (0.88 g) enable it to achieve a high speed–mass ratio of  $\approx 41 \text{ mm s}^{-1} \text{ g}^{-1}$ . Li et al. further proposed a variant based on an annular body made by the multi-segmented DEMES and six electroadhesive actuator (EAA) feet (Figure 5F).<sup>[65]</sup> The locomotion of this omnidirectional creeping robot (OCSR) is implemented through changing the shape of the annular body by activating different DE elements on the circular body, in combination with supporting adhesion provided by EAA feet in the creeping process (Figure 5G). One

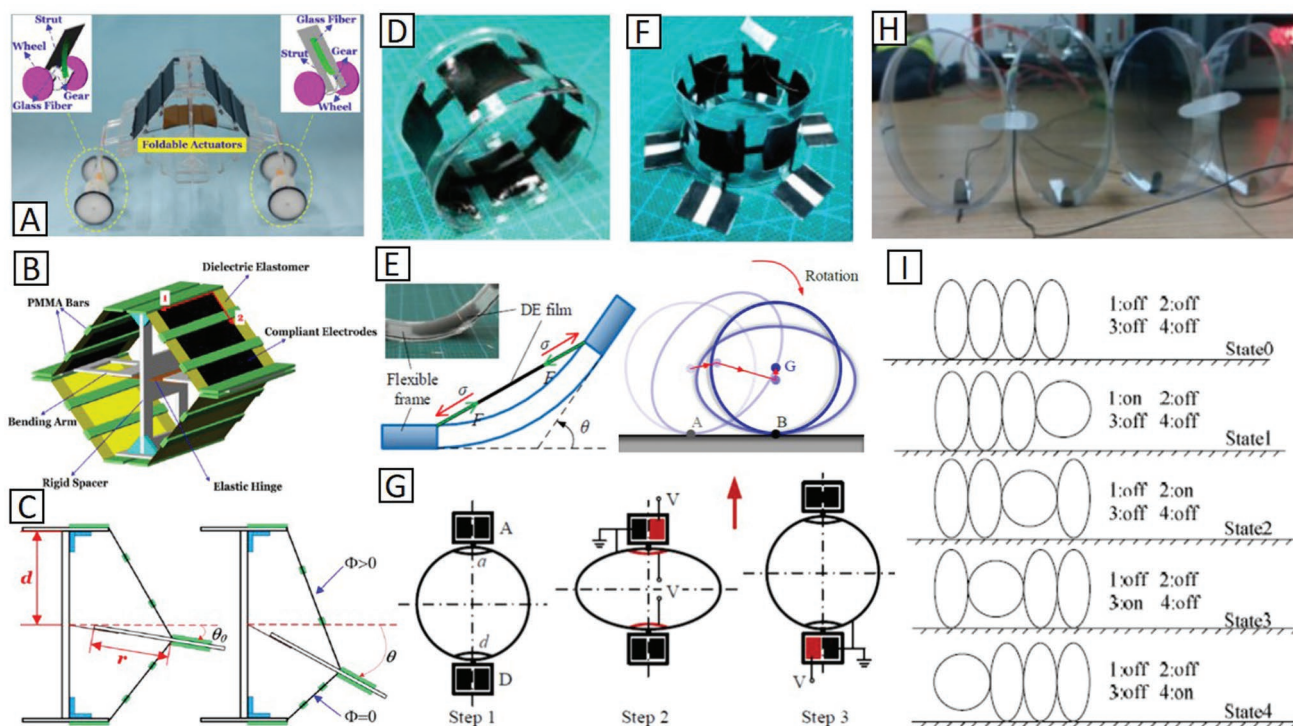


**Figure 5.** Soft crawling robots using closed-loop dielectric elastomers in rolling or sliding modes. A) A soft robot actuated by foldable DEAs, B) prototype of the enhanced foldable DEAs, and C) its operating principle. Reproduced with permission.<sup>[62]</sup> Copyright 2016, AIP. D) A rolling soft robot (RSR) based on the multisegment DEME, and E) stress state of an independent DEMES and rolling mechanism of RSR. Reproduced with permission.<sup>[30]</sup> Copyright 2018, IEEE. F) An omnidirectional creeping soft robot (OCSR) consisting of ADEA body and six EAA feet, and G) locomotion mechanism of OCSR. Reproduced with permission.<sup>[65]</sup> Copyright 2018, IOP. H) A creeping robot based on closed-loop DEA units, and I) locomotion mechanism. Reproduced with permission.<sup>[66]</sup> Copyright 2014, SPIE.

significant advantage of this design is its ease of control in the multidirectional movement.<sup>[28,54]</sup> The average speed along any of the creeping directions is 1.32–1.95 mm s<sup>-1</sup>, depending on the deformation mode of the annular body.

As illustrated in Figure 5H, a soft creeping robot is designed to have four closed-loop DE actuation units (AUs), which are fabricated by bonding a prestretched DE film onto an ellipse polyvinyl chloride (PVC) frame.<sup>[66]</sup> Initially, the recovery force from the PVC frame is smaller than the compression force applied by the prestretched DE film, resulting in an elliptical shape. When a voltage is applied, the DE film expands, making the frame restore its original circular shape and then pushing the adjacent AU forward. The DE film is prepared with a pre-strain of 300% × 300% to generate the largest length of short axis of the AU, that is 42 mm under 4.5 kV. As indicated in Figure 5I, the soft creeping robot can move forward in a cooperative manner by alternatively switching the shapes of AUs between ellipse and circle.

Figure 6A describes an inchworm-like untethered soft robot built by Cao et al.<sup>[6]</sup> This robot contains a deformable body made of DEAs (a two-layer film) and two paper-based feet equipped with EAAs (Figure 6B).<sup>[67]</sup> Two DE films are subject to equal-biaxial prestretches with carbon greases as electrodes,

sandwiched by two larger annular polyethylene terephthalate (PET) frames. This stacking structure forms a saddle-like shape without constraints and is capable of storing higher elastic energy through deformations. The expansion/contraction of DEAs and adhesion/detachment of EAAs are controlled by switching the voltages on/off, providing the locomotion forces for the inchworm-like motion. This locomotion process can be divided into three steps (Figure 6C): at first, a voltage is applied on the front foot, making it adhere to the surface. Then, the voltage applied on the front foot is switched off, while both the body and the rear foot are subjected to voltages. As a result, the front foot detaches while the rear foot remains attached, and DE body expands, leading to a forward motion of its front foot. Finally, the front foot is attached with the EAA turned on, and simultaneously the DE body shrinks to its original length and the rear foot detaches from the ground with applied voltages removed. This proposed design enables the soft robot to move forward or backward with high stability, even on uneven surfaces.<sup>[6]</sup>

To achieve large actuation strains and significant deformation, DE films usually require to be prestretched and applied to a high driving voltage,<sup>[27,68]</sup> which hinders their applications in soft robotics. To overcome this challenge, Duduta et al. developed a robot with four inchworm-like legs made of multilayered DEs

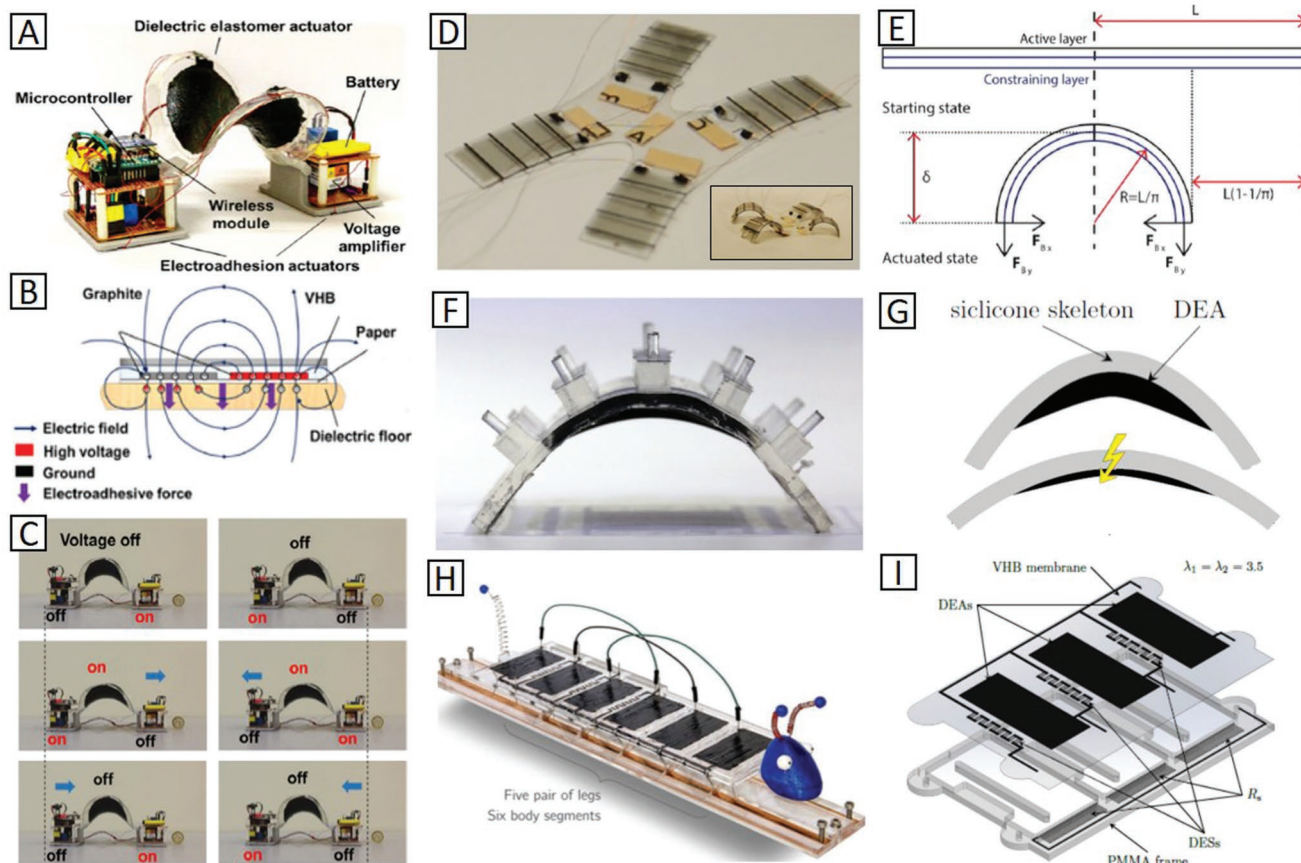


**Figure 6.** Soft inchworm-like crawling robots actuated by dielectric elastomers. A) A soft untethered robot built on the basis of the DEA and EAAs, B) mechanism of EAA, and C) translation mechanism of the untethered robot. Reproduced with permission.<sup>[28]</sup> Copyright 2018, Elsevier. D) A four-legged inchworm-like crawling robot, and E) its movement mechanism. Reproduced with permission.<sup>[27]</sup> Copyright 2017, IEEE. F) An entirely soft crawling robot made of DE, and G) its actuation mechanism. Reproduced with permission.<sup>[26]</sup> Copyright 2017, SPIE. H) The “Trevor” soft robot, and I) integrated configuration of DEO used in it. Reproduced with permission.<sup>[69]</sup> Copyright 2017, Mary Ann Liebert Inc.

driven by low voltages in a non-prestretched state (Figure 6D).<sup>[27]</sup> The inchworm-like leg can be modeled as the multilayer cantilever (Figure 6E). When a voltage is applied to the DE layers, the induced Maxwell stress in DE causes the cantilever to bend. With an electric field of  $50 \text{ V } \mu\text{m}^{-1}$  applied, the cantilever can be bent to be a semicircle shape. This bending deformation together with anisotropic friction drives the soft robot to move forward with the improved direction control ability. In another design of a soft crawling robot enabled by DEAs, a soft silicon skeleton, rather than rigid structures, has been used to retain the strain of the DE film (Figure 6F).<sup>[26]</sup> This silicone film is prestretched using an iris-like stretching rig made of polymethyl methacrylate (PMMA). Its locomotion mechanism is similar to that of an inchworm (Figure 6G). In brief, the prestretched DE film is first bonded to a silicon structure with an anisotropic bending stiffness. Then, the force induced by the prestrain in the membrane bends the whole-body along its softer axis. Once a high voltage is applied to the DE, the bending curvature of the structure will change, leading to the crawling motion of the robot via friction.

The use of either stretchable and/or miniaturized electronics or electronics-free design is of the utmost significance. However, most of the DEA-based soft robotics are not exclusively soft, as they require external electronic components including the control and power sources. Henke et al. designed the first electronics-free caterpillar-like soft robot—Trevor, made of polymer and carbon materials and structured with six body segments and five pairs of legs (Figure 6H).<sup>[69]</sup> The DEA works together with a dielectric elastomer switch (DES) in a side-by-side manner to generate a strain-dependent electrical signal inverter, and a self-oscillating dielectric elastomer oscillator (DEO) is developed by implementing a closed loop of an uneven number of inverters. The last three DE-based segments, including three “master” DEAs and three DESs, make DEO an active signal generator, while the first three segments are “slave” DEAs (Figure 6I). The in-plane motion of the six DEAs is converted into the forward motion through V-shaped compliant legs, each of which is connected to two adjacent DE films. This strain-coupled DES can deliver both the signal and excitatory charge for actuation, providing a self-regulating system. When a voltage is applied to one of the DEAs, it elongates and the DE film in the corresponding segment loses its tension, resulting in an up and forward motion of the leg beneath the activated DEA. It is noted that other applications of DE films as sensors,<sup>[70]</sup> charge controllers,<sup>[71]</sup> information processors,<sup>[72]</sup> power electronics, and harvesters<sup>[73]</sup> also have the potential to be integrated for the development of soft crawling robotic systems.

### 3.2. Shape Memory Alloys

SMA has been widely employed for fabricating soft robots owing to its high work density, large recovery stress and strain, silent operation, low stimulating voltage, corrosion resistance, and biocompatibility.<sup>[74–76]</sup> A deformed SMA object can restore its original shape when heated to its transition temperature due to the reversible diffusion-less conversion between states of starting austenite and post-deformation martensite phases.<sup>[74]</sup> SMA actuators are able to provide both the actuation and structural functionalities (e.g., the form of spring or meandering

profile).<sup>[75]</sup> However, they typically require high current, exhibit limited bandwidth, and have wide time windows to be cooled down. As illustrated in Figure 7A, an innovative soft robot—GoQBot is made of two independent SMA springs coupled with elastomeric materials, resembling a caterpillar and mimicking its movement, such as ballistic rolling and crawling.<sup>[20]</sup> Possessing a domed cross-section, solid material on the dorsa, and small wedge-shaped legs, GoQBot can perform ventralward body bending. In addition, the laterally elongated hammer head and the softer layer of sticky rubber improve its surface contact. To realize ballistic rolling, a firm pivoting anchor is required to produce the thrust. The hammer head and tail skids of this robot work as the terminal prolegs and thoracic legs; therefore, when SMA coils are heated, the dynamic body curling generates forward angular momentum around the head of the robot which functions as an anchor, curling this robot ballistically into a wheeling state and pushing it off.

Umedachi et al. also developed a caterpillar-like robot by using multimaterial 3D printing (Figure 7B).<sup>[75]</sup> Two coiled SMAs are tactfully embedded in robot's body and can be actuated electrically (Figure 7C). By arranging the two SMA actuators side-by-side and in an overlapped manner, a retrograde wave can be generated by contracting one of the SMA coils, and then the elastomeric body transfers the produced force to the other part of the body. The two SMA coils in such arrangement are able to stir up waves with different frequencies, wavelengths, phases, and amplitudes, generating multiple locomotion gaits based on interfacing of waves through robot's body. In addition, the variable frictional legs allow it to produce enough frictional forces via deforming the body to get the appropriate locomotion. Similarly, inspired by starfishes, a multirayed silicone-based robot was built with SMA (Figure 7D).<sup>[76]</sup> When the SMA spring is heated, the induced forward friction shifts the gravity center of the robot to form a stable shape, and then the opposite group of rays deform to store elastic potential energy and further push the robot ahead when releasing the energy (Figure 7E). Through repeated deformations of the rays induced by SMA actuator, continuous motion, including steering due to embedded independent actuation unit, can be achieved even in various terrain conditions.

Kim et al. designed a turtle-like robot with SMA-based smart soft composite (SSC) (Figure 7F).<sup>[77]</sup> The SSC structure consists of a series of active parts (SMA wires) generating actuation forces, with the passive parts (stiffen anisotropic material) controlling the angles of twisting and bending, and a polymeric matrix for combination and stiffness adjustment. Based on classic laminate theory and chain algorithm,<sup>[77]</sup> the force and momenta generated by the SSC structures are solved under various arrangements (angle-ply or cross-ply) to induce targeted locomotion. For instance, a positive ply-angles scaffold is utilized for posterior positive and interior negative twisting angles of the turtle flippers during upstroke and downstroke, respectively (Figure 7G).

Remarkably, Koh and Cho fabricated an omega-shaped inchworm-inspired crawling soft robot (Omegabot) using SMA coil-spring actuators (Figure 7H).<sup>[78]</sup> The soft Omegabot is made of a single piece of a composite comprising two four-bar linkages functioning as the bending segments, one spherical six-bar linkage as steering controller, and two anisotropic friction

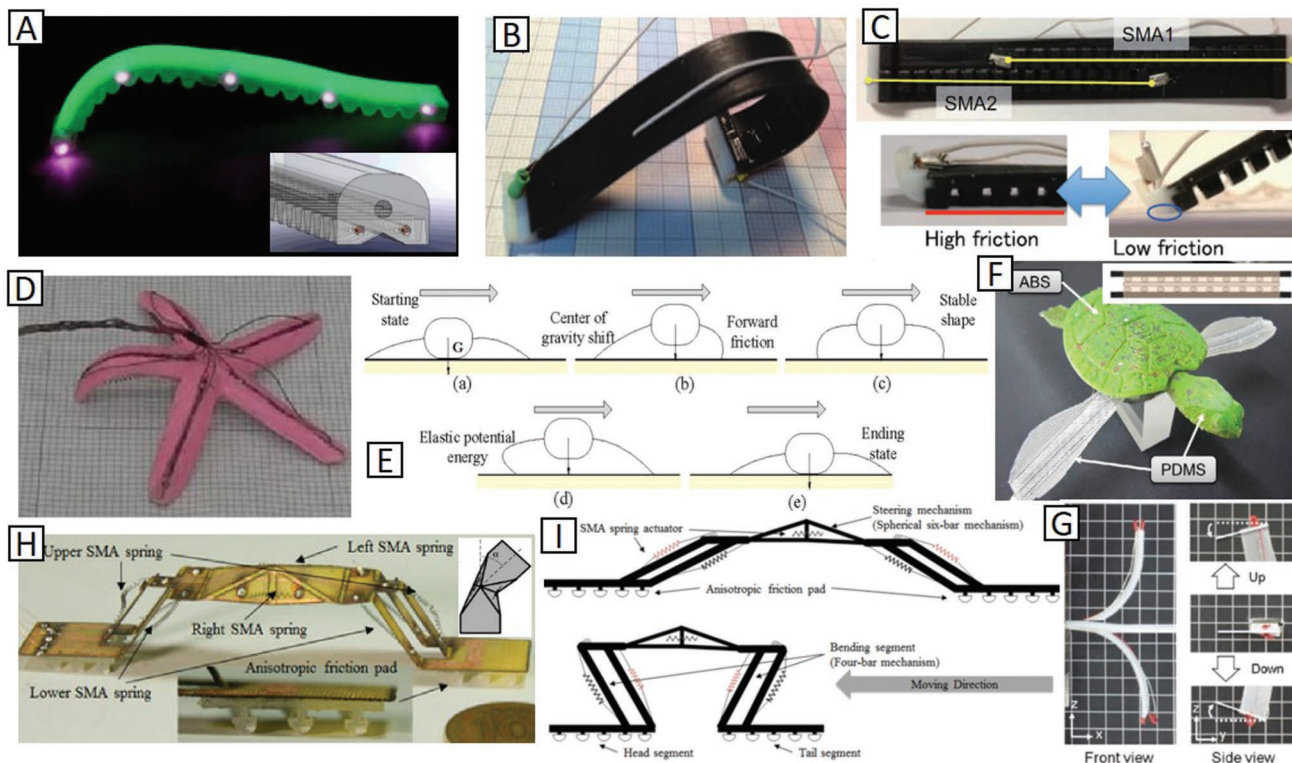


**Figure 7.** Soft crawling robots actuated by shape memory alloys. A) The design of GoQBot. Reproduced with permission.<sup>[20]</sup> Copyright 2011, IOP. B) A crawling and inching soft robot, and C) the SMA arrangement for it. Reproduced with permission.<sup>[75]</sup> Copyright 2013, IEEE. D) A starfish-like robot, and E) mechanism for crawling. Reproduced with permission.<sup>[76]</sup> Copyright 2013, IEEE. F) A turtle-like robot realized by SMA-based SSC actuators, and G) its conceptual swimming mechanism. Reproduced with permission.<sup>[77]</sup> Copyright 2012, IOP. H) Omegabot prototype with SMA springs and anisotropic friction pads, and I) schematic illustration of its prototype. Reproduced with permission.<sup>[78]</sup> Copyright 2013, IEEE.

pads made of soft materials (Figure 7I). The novel large pitch-angle range (LIP) SMA coil spring is designed to have a large spring index (11) and a pitch angle ( $29^\circ$ ) as well as improved cooling performance (0.3 s) due to more surrounding air compared to the traditional SMA springs. For crawling, the upper lower SMA springs are activated alternately. With this designed structure, the upper actuator extends the body while the lower actuator contracts it, leading to an omega shape of the robot. For steering, the spherical six-bar linkage is able to generate both pitch-axis and yaw-axis motions through driving the left and right SMA springs alternately. However, the Omegabot cannot move at a high frequency as the actuation frequency of the SMA spring is still limited by the inherent slow cooling down process. This Omegabot is lightweight (1.2 g in total body weight) and can be transported in microair vehicles to specific places for sensing and reconnaissance.

### 3.3. Magnetoactive Elastomers

MAEs are made by dispersing magnetic fillers into a soft elastomer matrix. In the presence of magnetic fields, soft MAEs are able to induce elongation, contraction, bending, or other kinds of deformations. The magnetization profile, actuating signal, and overall shape of filler materials, are the major parameters that affect the deformation patterns of such materials.<sup>[79]</sup> The

MAEs are ideal materials for soft robots targeting the applications in enclosed and confined spaces (e.g., microscale robots for biology).<sup>[32]</sup> **Figure 8A** shows a soft magnetic active robot capable of realizing desired time-varying shape change and multimodal locomotion exposure to magnetic fields.<sup>[80]</sup> Magnetic microparticles (neodymium–iron–boron, NdFeB) are dispersed in a silicon elastomer, and the high remnant magnetization and large coercivity of the NdFeB microparticles ensure the generation of effective magnetic actuation and guarantee the stability of magnetization profile during actuation. A uniform time-varying magnetic field can generate various locomotion modes, such as climbing, swimming, rolling, walking, and jumping, and can control the morphology of the robot and steer its locomotion in a specific direction. Furthermore, the as-fabricated robot can switch between locomotive modes, transit reversibly between different liquid and solid terrains, and can execute pick-and-place and cargo-release tasks.<sup>[80]</sup>

Remarkably, Lu et al. recently fabricated a soft multilegged millirobot based on a modified magnetic particle-assisted molding approach (Figure 8B).<sup>[21]</sup> These tapered feet structures are formed with a mixture comprising polydimethylsiloxane (PDMS), hexane, and magnetic particles under an external magnetic field. The magnetic field with distinct trajectory is added to achieve a combined discontinuous and continuous locomotion.<sup>[81]</sup> Under a controlled magnetic field, pulling force and magnetic torque are generated to deform the tapered feet align

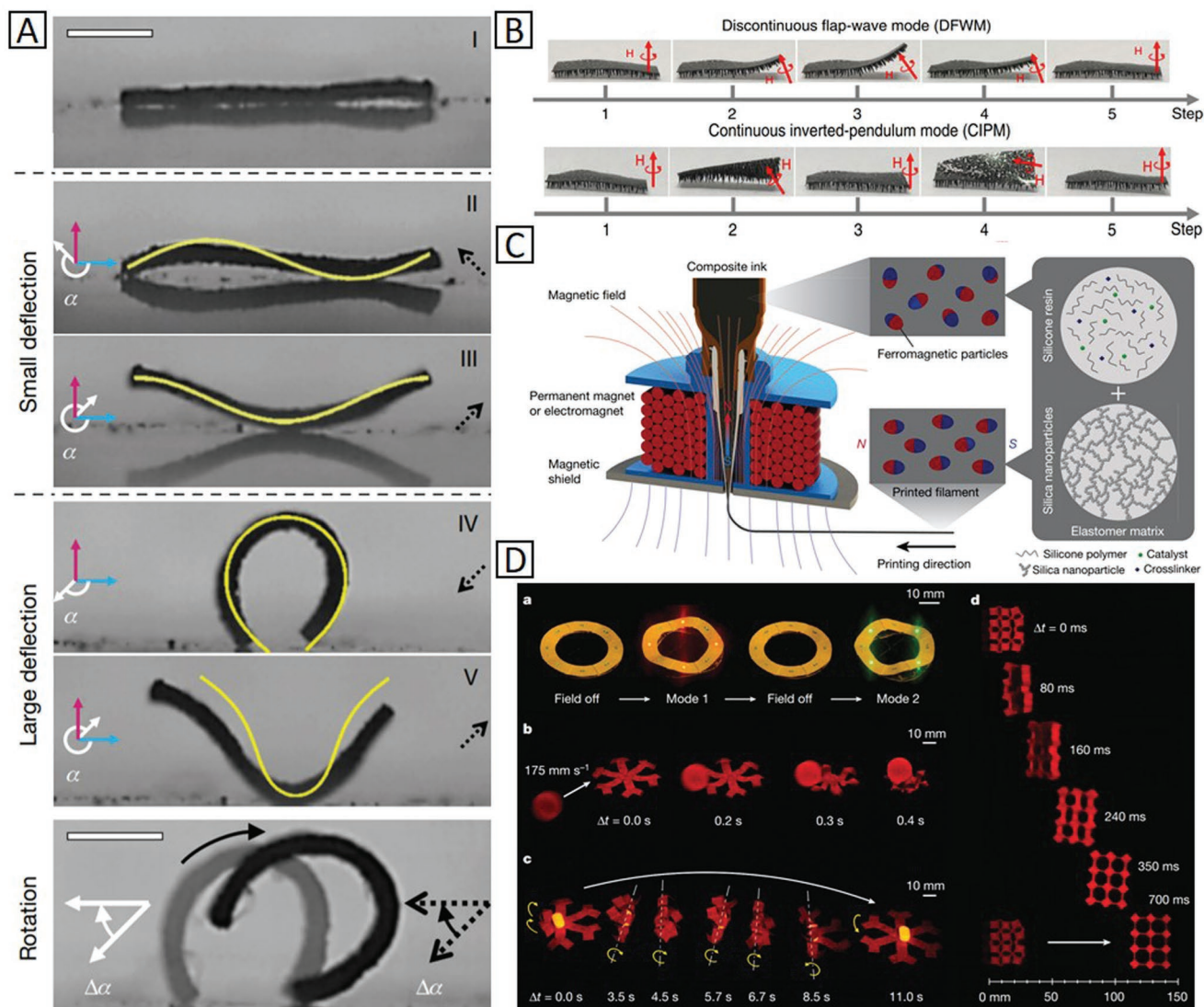


**Figure 8.** Soft crawling robots via magnetoactive elastomers. A) A small-scale soft robot capable of multimodal locomotion. Reproduced with permission.<sup>[80]</sup> Copyright 2018, SNG. B) A soft multilegged millirobot with two different locomotion modes. Reproduced with permission.<sup>[21]</sup> Copyright 2018, SNG. C) Schematics of material composition and printing process for fabricating an untethered fast-transforming soft robot and D) functional demonstrations of 3D-printed materials with programmed ferromagnetic domains: a) a reconfigurable electronic device exhibiting different electronic functions depending on magnetic field direction, b) a hexapedal structure stopping and holding a fast-moving object and c) taking a pharmaceutical pill and delivering to a specific location, and d) horizontal leap of a 3D auxetic structure upon sudden reversal of the applied magnetic field. Reproduced with permission.<sup>[83]</sup> Copyright 2018, SNG.

with the direction of magnetic flux, then to drive the robot crawling forward, as shown in Figure 8B.<sup>[82]</sup> Also, the storing and releasing of energy with flexible legs during locomotion decrease the total energy consumption while increase the stability and obstacle-traversal ability of the soft robot. The crawling millirobot made of MAE has demonstrated superior functionalities such as shape-changing, efficient locomotion, and load carrying.

In another recent study, Zhao and co-workers proposed the untethered fast-transforming soft materials via direct 3D printing with programmed ferromagnetic domains.<sup>[83]</sup> In their work, the ink is tailored by mixing magnetizable microparticles, silicon nanoparticles, and silicon rubber. During printing, a magnetic field is applied by an electromagnetic coil to the dispensing

nozzle, which can reorient the ferromagnetic particles to impart the patterned magnetic polarity to the extruded ink flow (Figure 8C). The capability of fabricating complex shapes and programmed ferromagnetic domains provide a variety of functions such as fast shape-shifting, stopping and holding a fast-moving object, as well as the ability to carry and to release objects with arbitrary shapes, demonstrating promising potential in flexible electronics, biomedical devices, and soft robotics (Figure 8D).

### 3.4. Liquid-Crystalline Elastomers

The LCEs are considered as promising active materials for soft actuators and soft robots due to their attractive flexibility and

self-organization feature. LCE consists of anisotropic mesogens (liquid crystal molecules) incorporated into polymer chains. The crosslinked liquid crystalline polymer (CLCP) transforms between liquid-crystalline and isotropic phases when exposed to a stimulus such as ultraviolet (UV), irradiation, or heat.<sup>[84]</sup> The liquid crystal molecule, crosslink density, and the connectivity of the mesogens to polymer chains affect the performance of an LCE actuator. Yamada et al. prepared a laminated film comprising a CLCP layer containing azobenzene moieties which can help in generating larger deformations, and a low-density polyethylene sheet to generate different locomotion modes by photoirradiation (Figure 9A).<sup>[85]</sup> In the smectic phase, the CLCP film exhibits a higher order of azobenzene mesogens along with the rubbing direction of the polyimide (PI) layer and can produce a larger force output. In addition, the CLCP film is able to work at room temperature due to the similar glass transition temperature. Because of the mismatched thermal expansion properties of the two laminated layers, the CLCP film will be curved. The initially curved laminated film becomes flat when exposed to the UV light and restores its original curved shape when triggered by a visible light irradiation, functioning as a “hinge joint” for locomotion (Figure 9B).<sup>[86]</sup> By controlling the irradiation wavelength, intensity, and the incident position to alternatively switch the stationary point, this multilayer film can move like an inchworm (Figure 9C). Rogó z et al. utilized a

similar approach to develop a natural scale caterpillar-like robot based on a single light sensitive LCE stripe (Figure 9D).<sup>[87]</sup> As illustrated in Figure 9E, a monomer mixture is laminated by two polyimide coated plates rubbed with a pattern of strips. This pattern is preserved by curing with UV irradiation, and the molecules are aligned along the rubbing direction at the rubbed regions, but randomly oriented in nonrubbed regions. As a result, the film appears flat when the temperature is lower than the phase transition temperature ( $T_{pt}$ ), while changing into a curved shape when heated above  $T_{pt}$  (Figure 9E). By scanning a laser beam from its tail to head, the robot is able to crawl forward (Figure 9F). The as-fabricated robot can squeeze through a narrow slit, walk up on a slope, or even push objects under light excitation with a moving speed of 0.1–0.5 mm s<sup>-1</sup>.

More recently, Wang et al. utilized a thermally responsive artificial muscle made of carbon-black-doped LCE (CB-LCE) nanocomposite to actuate an inchworm-like robot (Figure 9G).<sup>[22]</sup> In their design, a bimorph structure is built by sandwiching a heater between CB-LCE layer and Kapton film to mimic the “wavy” configuration of inchworms. A bending deformation can be triggered in the film when it is heated. As illustrated in Figure 9H, a synthetic robot fabricated by two electrically programmable bimorphs can move forward by alternatively turning the two heaters on and off with the front leg acting as a grip leading to anchor-pulling.

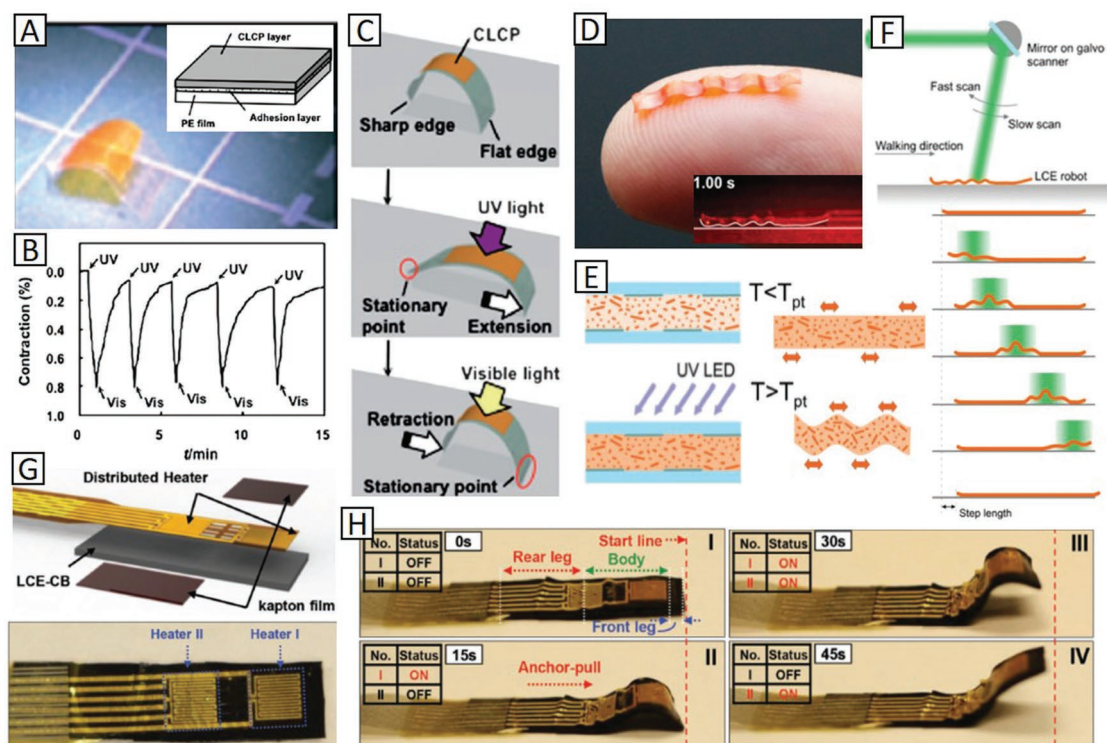


**Figure 9.** Soft crawling robots via liquid crystal elastomers. A) A soft crawling robot driven by a laminated CLCP film, B) alternating changes in length of the CLCP layer by irradiation with UV and visible light, and C) mechanism of the photoinduced inchworm walk of CLCP laminated film. Reproduced with permission.<sup>[85]</sup> Copyright 2009, Royal Society of Chemistry. D) A light driven caterpillar robot, E) fabrication of it by LCE film with patterned molecular orientation, and F) crawling locomotion mechanism via laser beam stimulation. Reproduced with permission.<sup>[87]</sup> Copyright 2016, Wiley-VCH. G) Structure of the crawling inchworm-like soft robot fabricated by LCE-CB, and H) sequential steps during one crawling stride moving forward of the robot. Reproduced with permission.<sup>[22]</sup> Copyright 2018, Wiley-VCH.

### 3.5. Piezoelectric Materials

PEMs are able to function as actuators when converting electricity into mechanical deformation through converse piezoelectric effect. Polyvinylidene fluoride (PVDF) is one of the most promising piezoelectric materials for soft robot applications, as it possesses superiority in thickness, weight, and flexibility, yet requires high driving voltages. For instance, a catapult origami with multilayered PVDF film can generate a  $19^\circ$  angular displacement under a voltage of 3 kV<sup>[88]</sup> and the space antennas can be controlled in the shape by applying a voltage of 0.8 kV.<sup>[89]</sup> Recently, Wu et al. developed a self-curved unimorph actuator by coating a thin layer of PVDF ( $d_{31} = -27 \text{ pC N}^{-1}$ ) film onto a prestretched PI tape with a thickness ratio of PVDF:PI = 2.5 (Figure 10A). Compared to the i) flat unimorph, this ii) curved structure can generate a larger deformation via a much lower driving voltage (200 V, peak to peak), and can alter its curvature based on the voltage applied (Figure 10B).<sup>[23]</sup> As depicted in Figure 10C, the precurved unimorph robot can crawl like an inchworm. When a maximum voltage (+100 V) is applied, the structure shrinks to its minimum curvature, having legs attached to the surface and the tail sliding forward (displacement of  $a_1$ ). When the voltage decreases to zero, the tail functions as an anchor while the legs move forward. When the voltage is reversed (-100 V), the body elongates to its smallest curvature and the tail attaches to the surface, after which the legs move forward (displacement of  $a_2$ ). As the amplitude of voltage tunes to zero again, the unimorph returns to its initial shape with the total displacement of  $a_1 + a_2$ . The as-fabricated inchworm robot achieves a speed of  $0.3 \text{ mm s}^{-1}$  on the paper surface, or  $1.9 \text{ mm s}^{-1}$  on a ratchet surface.

### 3.6. Ionic Polymer–Metal Composites

IPMCs, as a category of ionic electroactive polymers (EAPs) are typically composed of an ion-exchange membrane

(e.g., Flemion or Nafion), with its surface coated with metal electrodes (e.g., platinum, gold, and silver) chemically or physically. When a voltage is applied across the electrodes of a hydrated IPMC, the redistribution of charges will influence the hydrophilic regions in the polymer, leading to a fast bending deformation toward the anode side.<sup>[24]</sup> IPMCs have the advantages of lightweight, low actuation voltage (1–5 V), good flexibility, silent operation, and adaptability in the aquatic environment. Recently, Carrico et al. developed a modular IPMC robot inspired by caterpillars via the fused-filament 3D printing of IPMCs (Figure 11A).<sup>[90]</sup> The robot consists of modular ring-like legs which function as grippers and body units which act as extensors, capable of gripping and crawling along tubular structures. The body unit is made of an elliptically shaped IPMC actuator with four electrode regions on its interior and exterior surfaces. When a voltage is applied onto the anode connected to an exterior surface, the body unit will expand; however, when changing the polarity of voltage, it will contract (Figure 11B). Figure 11C shows the locomotion principle of the configuration with three legs and two body segments. Alternative expansion and contraction of these body segments along with the gripping and opening of legs can generate a wave-like motion traveling through the robot. It is demonstrated that this robot can crawl at a speed of  $\approx 0.157 \text{ mm s}^{-1}$ .

### 3.7. Twisted and Coiled Polymers

A new type of actuator was reported recently with its name given as, TCP or supercoiled polymer, based on its fabrication process.<sup>[91]</sup> This actuator is fabricated by twisting nylon threads (e.g., fishing line) into a coiled configuration. Normal type TCPs can be thermally actuated (contract under heat) to produce large strains and stresses. TCP actuators are promising for the soft robotics application due to their remarkable

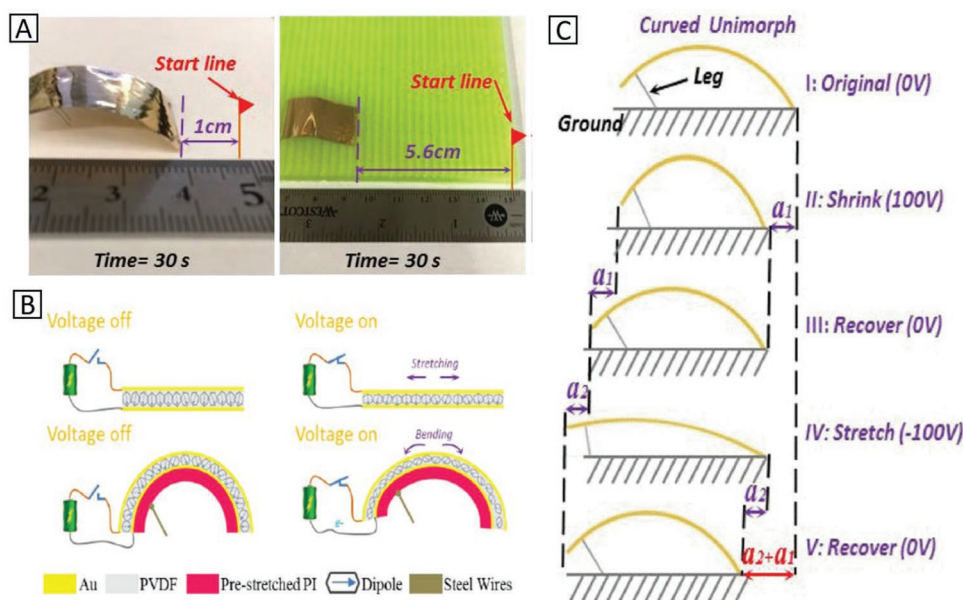


**Figure 10.** Soft crawling robots via piezoelectric materials. A) Locomotion of the curved PVDF-based soft robot crawling on two different surfaces, B) actuation principles of a PVDF film and a precurved composite layer (PVDF and PI), and C) a complete crawling process in one driving cycle based on the asymmetry friction on the right end of the design and the added legs on the left side. Reproduced with permission.<sup>[23]</sup> Copyright 2018, IEEE.

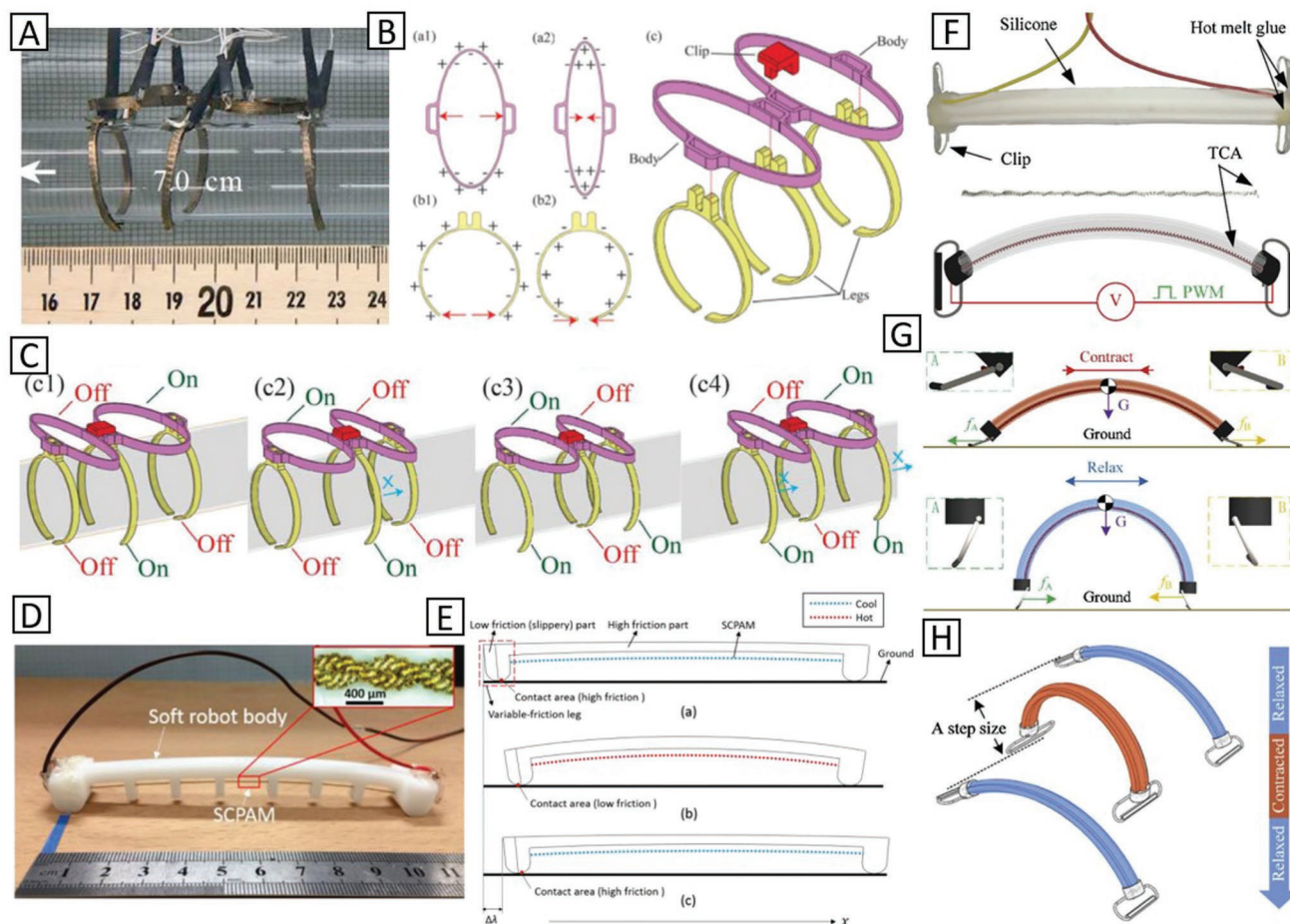


**Figure 11.** Soft crawling robots driven by ionic polymer–metal composites (IPMC) and twisted and coiled polymers. A) A soft crawling robot comprising three legs and two body units made of IPMC, B) actuations of the modular leg and body as well as the assembly of robot, and C) locomotion mechanism in a single cycle based on expansion/contraction of the body segment and the gripping and opening of the legs.<sup>[90]</sup> Copyright 2017, IEEE. D) An inchworm-like robot actuated by SCPAM, and E) locomotion process based on the bending of the body and the anisotropic friction.<sup>[92]</sup> Copyright 2019, IEEE. F) Structure of the soft crawling robot by a single TCP actuator, G) illustration of the locomotion mechanism of the TCP robots via friction change, and H) the locomotion process of the soft crawling robot.<sup>[93]</sup> Copyright 2019, Elsevier.

properties, such as lightweight, excellent flexibility, high energy density, long cycle life, small hysteresis, and low cost.<sup>[91]</sup> Furthermore, electric activation through Joule heating can be realized by utilizing conductive nylon fibers in TCPs, which is the most efficient approach to drive TCPs.<sup>[25]</sup> Recently, Yang et al. applied a supercoiled polymer artificial muscle (SCPAM) into a soft crawling robot (Figure 11D).<sup>[92]</sup> The main body of this robot is made of silicone rubber while the slippery part located at its edge is made of resin with a smaller friction coefficient, leading to a variable-friction leg (Figure 11E). When the SCPAM is heated, contraction induced by SCPAM will bend the robot's body over the threshold angle, and thus the slippery area will get in contact with the ground, pushing the robot's body forward. When the SCPAM is cooled down, the high friction area will prevent the robot from moving backward. This crawling robot with simple structures can attain an average speed of  $0.245 \text{ mm s}^{-1}$  on a wood surface when the SCPAM is actuated at  $0.16 \text{ W cm}^{-1}$ . In another study, Tang et al. developed a similar crawling robot based on a single TCP actuator (Figure 11F).<sup>[93]</sup> The bar-like body can be continuously bended through

actuating the nickel-wound TCP actuator embedded in the neutral axis of the robot. Anisotropic friction is implemented with the help of two special paper-based chips which serve as feet and the hot melt glue attached on them (Figure 11G). The outer side of foot A (left one) is coated with hot melt glue (a high friction coefficient) while the melt glue is applied to the inner side of the other foot. Based on the same locomotion mechanism discussed in Figure 11E, the robot can crawl at a speed of  $1.2 \text{ mm s}^{-1}$  by varying the temperature between 60 and  $100 \text{ }^\circ\text{C}$  with a period of 5 s.

#### 4. Summary and Outlook

In summary, we have reviewed recent advances in soft crawling robots, with the focus placed on the actuation, structural design, and locomotion mechanism, as well as their implementation and performance of the reported robots. The major actuation approaches have been discussed, including pneumatic/hydraulic actuation, chemical reaction actuation, and soft active

material-based actuation. For each actuation approach, we have discussed the advantages and drawbacks of each design. It should be noted that although significant progress has been made over the past decade, there remains many challenges that need to be addressed for improving the soft crawling robots. For instance, the fluidic (pneumatic and hydraulic) actuators require a supply of pressurized fluid as well as channels and tubes to transport fluids, which significantly constraint its response speed, working efficiency, and moving freedom. DEAs need complex stacks for linear contraction due to the limited strains and deformations generated, and they usually require a prestretched and rigid frame to perform efficiently. To solve these problems, novel multifunctional materials and structures will have to be developed in the future: Tough and self-healing materials that can withstand or self-repair when getting damaged to improve the durability of the soft crawling robots in unpredictable environments. Also, it will be useful to have crawling robots with tunable stiffness by combining phase change materials with electronic actuation or pressurization. In addition, untethered mobile robots that can be controlled remotely or operate autonomously for surgery, drug delivery, diagnostics, or imaging are of immense interest and represent a promising direction in the future. MAEs and LCEs may play critical roles in this field due to their unique user-friendly operation requirement and safe working conditions.

It is promising to combine multiple actuation mechanisms together for soft crawling robots to fully utilize the advantages of each actuation approach but avoid possible shortfalls of them. For example, we can couple the hydraulic and electrostatic actuators to achieve more efficient bending actuation. SMA-based actuators usually require longer time to cool down, imposing restrictions on bandwidth. A combination of soft fluidic actuators with SMA would be a good strategy to develop fast responsive and effective actuators for the propulsion of soft crawling robots. Moreover, there are no soft crawling robots of microscale or sub-millimeter size reported in literature. Most current soft crawling robots are generally big in volume, at millimeter or centimeter scale, and very difficult to be used in enclosed and confined spaces (e.g., blood vascular or intestinal tract) for disease diagnostic, therapy, or drug delivery, etc. It will be important and interesting to miniaturize the soft crawling robots to the sub-millimeter size scale for broadening their applications in biomedical engineering.

Another challenge and opportunity for soft crawling robotics comes from the integration of independent power supply for actuation. Most soft robots require electricity wires or fluid flow tubes for actuation power supply, which has significantly limited their use in many potential applications. Therefore, there is an urgent demand to develop self-powered soft crawling robots in the future. It would be helpful and important to integrate solar cells, triboelectric nanogenerators, or other energy harvesting mechanisms with soft robotics. Furthermore, by mimicking animals and insects, it is of interest to develop soft crawling robots capable of reconfiguration and loadbearing through properly integrating soft and rigid materials.

Autonomous locomotion is another challenge and opportunity for soft mobile robots to deal with complex environments. It will be highly desired to develop soft, flexible, or stretchable artificial skins for soft robots to provide tactile and sensing

capability, while offering real-time feedback for self-controlling and adjustment. On the other hand, although the soft body can relieve possible damage, the inaccurate actuation of soft robots increases the possibility for collision. Thus, developing distributed sensing elements has the potential to improve the situation and enable active morphology adaption. It is interesting to note that the requirement for soft robots on distributed sensing may be lower than rigid robots. For unstructured tasks such as explorations and rescues, “bang-bang” sensing may serve as an effective method for avoiding severe risks, leaving the rest to the soft body.

In addition, it will be helpful and valuable to develop fast prototyping methods that can easily integrate soft materials, fluid, and electronics into complex robotic structures. Due to the challenges raised by the complex nonlinear behaviors of soft bodies, efficient methods and techniques should be developed for the simulation and control of the new prototypes of soft crawling robots to facilitate their development and optimization. It is expected that with the advances in material development, novel designs, and innovative actuation and propulsion mechanisms, soft crawling robots will be able to find practical use in a broad range of applications in the future.

## Acknowledgements

S.C. and Y.C. contributed equally to this work. This work was supported in part by the USDA National Institute of Food and Agriculture Hatch Project (No. 1016788) and the Michigan State University Strategic Partnership Grant (16-SPG-Full-3236).

## Conflict of Interest

The authors declare no conflict of interest.

## Keywords

locomotion, soft active materials, soft actuators, soft crawling robots, soft robotics

Received: September 23, 2019

Revised: November 7, 2019

Published online:

- 
- [1] a) F. Iida, C. Laschi, *Procedia Comput. Sci.* **2011**, *7*, 99;  
b) M. T. Tolley, R. F. Shepherd, B. Mosadegh, K. C. Galloway, M. Wehner, M. Karpelson, R. J. Wood, G. M. Whitesides, *Soft Rob.* **2014**, *1*, 213.  
[2] B. Trimmer, *Soft Rob.* **2015**, *2*, 1.  
[3] S. Kim, C. Laschi, B. Trimmer, *Trends Biotechnol.* **2013**, *31*, 287.  
[4] D. Rus, M. T. Tolley, *Nature* **2015**, *521*, 467.  
[5] A. A. Stokes, R. F. Shepherd, S. A. Morin, F. Ilievski, G. M. Whitesides, *Soft Rob.* **2014**, *1*, 70.  
[6] J. Cao, L. Qin, J. Liu, Q. Ren, C. C. Foo, H. Wang, H. P. Lee, J. Zhu, *Extreme Mech. Lett.* **2018**, *21*, 9.  
[7] a) E. J. Van Henten, J. Hemming, B. Van Tuijl, J. Kornet, J. Meuleman, J. Bontsema, E. Van Os, *Auton. Rob.* **2002**, *13*, 241;  
b) A. J. Davison, I. D. Reid, N. D. Molton, O. Stasse, *IEEE Trans.*

- Pattern Anal. Mach. Intell.* **2007**, 29, 1052; c) S. Soatto, R. Frezza, P. Perona, *IEEE Trans. Autom. Control* **1996**, 41, 393.
- [8] N. Tan, R. E. Mohan, A. Watanabe, *Autom. Constr.* **2016**, 69, 68.
- [9] H. Seraji, A. Howard, *IEEE Trans. Rob. Autom.* **2002**, 18, 308.
- [10] R. F. Shepherd, F. Ilievski, W. Choi, S. A. Morin, A. A. Stokes, A. D. Mazzeo, X. Chen, M. Wang, G. M. Whitesides, *Proc. Natl. Acad. Sci. USA* **2011**, 108, 20400.
- [11] a) M. Calisti, M. Giorelli, G. Levy, B. Mazzolai, B. Hochner, C. Laschi, P. Dario, *Bioinspiration Biomimetics* **2011**, 6, 036002; b) T. Manwell, B. Guo, J. Back, H. Liu, in *2018 IEEE Int. Conf. on Soft Robotics (RoboSoft)*, IEEE, Piscataway, NJ **2018**, pp. 54–59; c) J. Yu, J. Xiao, X. Li, W. Wang, *Int. J. Adv. Rob. Syst.* **2016**, 13, 1.
- [12] a) C. Laschi, B. Mazzolai, M. Cianchetti, *Sci. Rob.* **2016**, 1, eaah3690; b) M. Calisti, G. Picardi, C. Laschi, *J. R. Soc., Interface* **2017**, 14, 20170101; c) M. Cianchetti, C. Laschi, A. Menciassi, P. Dario, *Nat. Rev. Mater.* **2018**, 3, 143.
- [13] S. I. Rich, R. J. Wood, C. Majidi, *Nat. Electron.* **2018**, 1, 102.
- [14] K. M. Digumarti, C. Cao, J. Guo, A. T. Conn, J. Rossiter, in *2018 IEEE Int. Conf. on Soft Robotics (RoboSoft)*, IEEE, Piscataway, NJ **2018**, pp. 303–308.
- [15] R. MacCurdy, R. Katschmann, Y. Kim, D. Rus, in *2016 IEEE Int. Conf. on Robotics and Automation (ICRA)*, IEEE, Piscataway, NJ **2016**, pp. 3878–3885.
- [16] N. W. Bartlett, M. T. Tolley, J. T. B. Overvelde, J. C. Weaver, B. Mosadegh, K. Bertoldi, G. M. Whitesides, R. J. Wood, *Science* **2015**, 349, 161.
- [17] H. Shen, *Nature* **2016**, 530, 24.
- [18] M. Wehner, R. L. Truby, D. J. Fitzgerald, B. Mosadegh, G. M. Whitesides, J. A. Lewis, R. J. Wood, *Nature* **2016**, 536, 451.
- [19] G.-Y. Gu, J. Zhu, L.-M. Zhu, X. Zhu, *Bioinspiration Biomimetics* **2017**, 12, 011003.
- [20] H.-T. Lin, G. G. Leisk, B. Trimmer, *Bioinspiration Biomimetics* **2011**, 6, 026007.
- [21] H. Lu, M. Zhang, Y. Yang, Q. Huang, T. Fukuda, Z. Wang, Y. Shen, *Nat. Commun.* **2018**, 9, 3944.
- [22] C. Wang, K. Sim, J. Chen, H. Kim, Z. Rao, Y. Li, W. Chen, J. Song, R. Verduzco, C. Yu, *Adv. Mater.* **2018**, 30, 1706695.
- [23] Y. Wu, K. Y. Ho, K. Kariya, R. Xu, W. Cai, J. Zhong, Y. Ma, M. Zhang, X. Wang, L. Lin, in *2018 IEEE Micro Electro Mechanical Systems (MEMS)*, IEEE, Piscataway, NJ **2018**, pp. 581–584.
- [24] M. Shahinpoor, K. J. Kim, *Smart Mater. Struct.* **2001**, 10, 819.
- [25] S. M. Mirvakili, A. R. Ravandi, I. W. Hunter, C. S. Haines, N. Li, J. Foroughi, S. Naficy, G. M. Spinks, R. H. Baughman, J. D. Madden, in *Electroactive Polymer Actuators and Devices (EAPAD) 2014* (Ed: Y. Bar-Cohen), Vol. 9056, SPIE, Bellingham, WA **2014**, pp. 77–86.
- [26] E.-F. M. Henke, K. E. Wilson, I. A. Anderson, in *Electroactive Polymer Actuators and Devices (EAPAD) 2017* (Ed: Y. Bar-Cohen), Vol. 10163, SPIE, Bellingham, WA **2017**, pp. 287–297.
- [27] M. Duduta, D. R. Clarke, R. J. Wood, in *2017 IEEE Int. Conf. on Robotics and Automation (ICRA)*, IEEE, Piscataway, NJ **2017**, pp. 4346–4351.
- [28] J. Cao, L. Qin, H. P. Lee, J. Zhu, in *Electroactive Polymer Actuators and Devices (EAPAD) 2017* (Ed: Y. Bar-Cohen), Vol. 10163, SPIE, Bellingham, WA **2017**, pp. 322–328.
- [29] C. Branyan, C. Fleming, J. Remaley, A. Kothari, K. Tumer, R. L. Hatton, Y. Mengüç, in *2017 IEEE Int. Conf. on Robotics and Biomimetics (ROBIO)*, IEEE, Piscataway, NJ **2017**, pp. 282–289.
- [30] W. B. Li, W. M. Zhang, H. X. Zou, Z. K. Peng, G. Meng, *IEEE/ASME Trans. Mechatronics* **2018**, 23, 1630.
- [31] J. Shintake, V. Cacucciolo, D. Floreano, H. Shea, *Adv. Mater.* **2018**, 30, 1707035.
- [32] L. Hines, K. Petersen, G. Z. Lum, M. Sitti, *Adv. Mater.* **2017**, 29, 1603483.
- [33] B. Mosadegh, P. Polygerinos, C. Keplinger, S. Wennstedt, R. F. Shepherd, U. Gupta, J. Shim, K. Bertoldi, C. J. Walsh, G. M. Whitesides, *Adv. Funct. Mater.* **2014**, 24, 2163.
- [34] F. Ilievski, A. D. Mazzeo, R. F. Shepherd, X. Chen, G. M. Whitesides, *Angew. Chem., Int. Ed.* **2011**, 50, 1890.
- [35] a) H. Lissmann, *J. Exp. Biol.* **1950**, 26, 368; b) H. Marvi, J. P. Cook, J. L. Streator, D. L. Hu, *Biotribology* **2016**, 5, 52; c) D. L. Hu, J. Nirody, T. Scott, M. J. Shelley, *Proc. Natl. Acad. Sci. USA* **2009**, 106, 10081; d) Y. Cao, Y. Liu, Y. Chen, L. Zhu, Y. Yan, X. Chen, *J. Mech. Phys. Solids* **2017**, 99, 304.
- [36] a) H. A. Abdel-Aal, M. El Mansori, *Surf. Topogr.: Metrol. Prop.* **2013**, 1, 015001; b) H. Marvi, Y. Han, M. Sitti, *Appl. Phys. Lett.* **2015**, 106, 051602; c) S. Das, N. Cadirov, S. Chary, Y. Kaufman, J. Hogan, K. L. Turner, J. N. Israelachvili, *J. R. Soc., Interface* **2015**, 12, 20141346; d) T. Yamaguchi, Y. Sawae, S. M. Rubinstein, *Extreme Mech. Lett.* **2016**, 9, 331.
- [37] A. Rafsanjani, Y. Zhang, B. Liu, S. M. Rubinstein, K. Bertoldi, *Sci. Rob.* **2018**, 3, eaar7555.
- [38] a) T. C. Shyu, P. F. Damasceno, P. M. Dodd, A. Lamoureux, L. Xu, M. Shlian, M. Shtein, S. C. Glotzer, N. A. Kotov, *Nat. Mater.* **2015**, 14, 785; b) M. K. Bles, A. W. Barnard, P. A. Rose, S. P. Roberts, K. L. McGill, P. Y. Huang, A. R. Ruyack, J. W. Kevek, B. Kobrin, D. A. Muller, *Nature* **2015**, 524, 204; c) A. Rafsanjani, K. Bertoldi, *Phys. Rev. Lett.* **2017**, 118, 084301; d) Y. Tang, G. Lin, S. Yang, Y. K. Yi, R. D. Kamien, J. Yin, *Adv. Mater.* **2017**, 29, 1604262.
- [39] M. A. Robertson, J. Paik, *Sci. Rob.* **2017**, 2, eaan6357.
- [40] M. S. Verma, A. Ainla, D. Yang, D. Harburg, G. M. Whitesides, *Soft Rob.* **2018**, 5, 133.
- [41] D. Yang, M. S. Verma, J. H. So, B. Mosadegh, C. Keplinger, B. Lee, F. Khashai, E. Lossner, Z. Suo, G. M. Whitesides, *Adv. Mater. Technol.* **2016**, 1, 1600055.
- [42] A. Ainla, M. S. Verma, D. Yang, G. M. Whitesides, *Soft Rob.* **2017**, 4, 297.
- [43] H. Ahmadzadeh, E. Masehian, M. Asadpour, *J. Intell. Rob. Syst.* **2016**, 81, 317.
- [44] J. Zou, Y. Lin, C. Ji, H. Yang, *Soft Rob.* **2018**, 5, 164.
- [45] A. Jacobson, *Tribol. Lubr. Technol.* **2004**, 60, 30.
- [46] M. Chua, R. Yeow, *Robotics* **2017**, 6, 34.
- [47] M. De Volder, D. Reynaerts, *J. Micromech. Microeng.* **2010**, 20, 043001.
- [48] a) C. D. Onal, X. Chen, G. M. Whitesides, D. Rus, in *Robotics Research* (Eds: H. Christensen, O. Khatib), Springer, Cham, Switzerland **2017**, p. 525; b) M. Wehner, M. T. Tolley, Y. Mengüç, Y.-L. Park, A. Mozeika, Y. Ding, C. Onal, R. F. Shepherd, G. M. Whitesides, R. J. Wood, *Soft Rob.* **2014**, 1, 263.
- [49] B. Mosadegh, C.-H. Kuo, Y.-C. Tung, Y.-s. Torisawa, T. Bersano-Begey, H. Tavana, S. Takayama, *Nat. Phys.* **2010**, 6, 433.
- [50] R. Pelrine, Q. Pei, R. Kornbluh, in *Electroactive Polymer Actuators and Devices (EAPAD) XX* (Ed: Y. Bar-Cohen), Vol. 10594, SPIE, Bellingham, WA **2018**, pp. 15–22.
- [51] T. Mirfakhrai, J. D. Madden, R. H. Baughman, *Mater. Today* **2007**, 10, 30.
- [52] R. D. Kornbluh, R. Pelrine, Q. Pei, R. Heydt, S. Stanford, S. Oh, J. Eckerle, in *Smart Structures and Materials 2002: Industrial and Commercial Applications of Smart Structures Technologies* (Ed: A.-M. R. McGowan), Vol. 4698, SPIE, Bellingham, WA **2002**, pp. 254–270.
- [53] J. Eckerle, S. Stanford, J. Marlow, R. Schmidt, S. Oh, T. Low, S. V. Shastri, in *Smart Structures and Materials 2001: Industrial and Commercial Applications of Smart Structures Technologies* (Ed: A.-M. R. McGowan), Vol. 4332, SPIE, Bellingham, WA **2001**, pp. 269–280.
- [54] R. Pelrine, R. D. Kornbluh, Q. Pei, S. Stanford, S. Oh, J. Eckerle, R. J. Full, M. A. Rosenthal, K. Meijer, in *Smart Structures and*

- Materials 2002: Electroactive Polymer Actuators and Devices (EAPAD)* (Ed: Y. Bar-Cohen), Vol. 4695, SPIE, Bellingham, WA **2002**, pp. 126–137.
- [55] a) Q. Pei, R. Pelrine, S. Stanford, R. D. Kornbluh, M. S. Rosenthal, K. Meijer, R. J. Full, in *Smart Structures and Materials 2002: Industrial and Commercial Applications of Smart Structures Technologies* (Ed: A.-M. R. McGowan), Vol. 4698, SPIE, Bellingham, WA **2002**, pp. 246–253; b) Q. Pei, M. Rosenthal, S. Stanford, H. Prahlad, R. Pelrine, *Smart Mater. Struct.* **2004**, *13*, N86.
- [56] C. T. Nguyen, H. Phung, T. D. Nguyen, C. Lee, U. Kim, D. Lee, H. Moon, J. Koo, J. D. Nam, H. R. Choi, *Smart Mater. Struct.* **2014**, *23*, 065005.
- [57] N. H. Chuc, N. H. L. Vuong, D. S. Kim, H. P. Moon, J. C. Koo, Y. K. Lee, J.-D. Nam, H. R. Choi, *IEEE/ASME Trans. Mechatronics* **2011**, *16*, 167.
- [58] C. T. Nguyen, H. Phung, H. Jung, U. Kim, T. D. Nguyen, J. Park, H. Moon, J. C. Koo, H. R. Choi, in *2015 IEEE Int. Conf. on Robotics and Automation (ICRA)*, IEEE, Piscataway, NJ **2015**, pp. 4484–4489.
- [59] C. T. Nguyen, H. Phung, P. T. Hoang, T. D. Nguyen, H. Jung, H. Moon, J. C. Koo, H. R. Choi, in *2017 IEEE/RSJ Int. Conf. on Intelligent Robots and Systems (IROS)*, IEEE, Piscataway, NJ **2017**, pp. 6233–6238.
- [60] a) H. Choi, K. M. Jung, J. W. Kwak, S. W. Lee, H. Kim, J. W. Jeon, J. D. Nam, in *Smart Structures and Materials 2003: Electroactive Polymer Actuators and Devices (EAPAD)* (Ed: Y. Bar-Cohen), Vol. 5051, SPIE, Bellingham, WA **2003**, pp. 262–271; b) H. Choi, K. M. Jung, J. Kwak, S. Lee, H. Kim, J. W. Jeon, J. Nam, in *2003 IEEE Int. Conf. on Robotics and Automation*, IEEE, Piscataway, NJ **2003**, pp. 1857–1862.
- [61] R. H. Armour, J. F. Vincent, *J. Bionic Eng.* **2006**, *3*, 195.
- [62] W. Sun, F. Liu, Z. Ma, C. Li, J. Zhou, *J. Appl. Phys.* **2016**, *120*, 084901.
- [63] a) J. Shintake, S. Rosset, B. E. Schubert, D. Floreano, H. R. Shea, *IEEE/ASME Trans. Mechatronics* **2015**, *20*, 1997; b) K. B. Subramani, E. Cakmak, R. J. Spontak, T. K. Ghosh, *Adv. Mater.* **2014**, *26*, 2949; c) T. Lu, Z. Suo, J. Huang, J. Zhu, D. Clarke, *Appl. Phys. Lett.* **2012**, *100*, 211901.
- [64] a) J. Sastra, S. Chitta, M. Yim, *Int. J. Rob. Res.* **2009**, *28*, 758; b) M. Artusi, M. Potz, J. Aristizabal, C. Menon, S. Cocuzza, S. Debei, *IEEE/ASME Trans. Mechatronics* **2011**, *16*, 50; c) A. Firouzeh, M. Ozmaeian, A. Alasty, A. I. Zad, *Smart Mater. Struct.* **2012**, *21*, 065011.
- [65] W.-B. Li, W.-M. Zhang, H.-X. Zou, Z.-K. Peng, G. Meng, *Smart Mater. Struct.* **2018**, *27*, 115024.
- [66] J. Zhao, J. Niu, L. Liu, J. Yu, in *Electroactive Polymer Actuators and Devices (EAPAD) 2014* (Ed: Y. Bar-Cohen), Vol. 9056, SPIE, Bellingham, WA **2014**, pp. 40–45.
- [67] a) M. A. Graule, P. Chirarattananon, S. B. Fuller, N. T. Jafferis, K. Y. Ma, M. Spenko, R. Kornbluh, R. J. Wood, *Science* **2016**, *352*, 978; b) A. Yamamoto, T. Nakashima, T. Higuchi, in *2007 Int. Symp. on Micro-NanoMechatronics and Human Science*, IEEE, Piscataway, NJ **2007**, pp. 389–394.
- [68] M. Duduta, R. J. Wood, D. R. Clarke, *Adv. Mater.* **2016**, *28*, 8058.
- [69] E. F. M. Henke, S. Schlatter, I. A. Anderson, *Soft Rob.* **2017**, *4*, 353.
- [70] a) L. A. Toth, A. A. Goldenberg, in *Smart Structures and Materials 2002: Electroactive Polymer Actuators and Devices (EAPAD)* (Ed: Y. Bar-Cohen), Vol. 4695, SPIE, Bellingham, WA **2002**, pp. 323–334; b) T. Gisby, S. Xie, E. Calius, I. Anderson, in *Electroactive Polymer Actuators and Devices (EAPAD) 2009* (Eds: Y. Bar-Cohen, T. Wallmersperger), Vol. 7287, SPIE, Bellingham, WA **2009**, pp. 72–83.
- [71] B. M. O'Brien, E. P. Calius, T. Inamura, S. Q. Xie, I. A. Anderson, *Appl. Phys. A: Mater. Sci. Process.* **2010**, *100*, 385.
- [72] B. M. O'Brien, I. A. Anderson, *Appl. Phys. Lett.* **2013**, *102*, 104102.
- [73] B. O'Brien, T. McKay, E. Calius, I. Anderson, *Appl. Phys. Lett.* **2011**, *98*, 142903.
- [74] D. Dye, *Nat. Mater.* **2015**, *14*, 760.
- [75] T. Umedachi, V. Vikas, B. A. Trimmer, in *2013 IEEE/RSJ Int. Conf. on Intelligent Robots and Systems (IROS)*, IEEE, Piscataway, NJ **2013**, pp. 4590–4595.
- [76] S. Mao, E. Dong, M. Xu, H. Jin, F. Li, J. Yang, in *2013 IEEE Int. Conf. on Robotics and Biomimetics (ROBIO)*, IEEE, Piscataway, NJ **2013**, pp. 91–96.
- [77] H.-J. Kim, S.-H. Song, S.-H. Ahn, *Smart Mater. Struct.* **2013**, *22*, 014007.
- [78] J.-S. Koh, K.-J. Cho, *IEEE/ASME Trans. Mechatronics* **2013**, *18*, 419.
- [79] a) B. J. Nelson, I. K. Kaliakatsos, J. J. Abbott, *Annu. Rev. Biomed. Eng.* **2010**, *12*, 55; b) M. Sitti, H. Ceylan, W. Hu, J. Giltinan, M. Turan, S. Yim, E. Diller, *Proc. IEEE* **2015**, *103*, 205; c) G. Z. Lum, Z. Ye, X. Dong, H. Marvi, O. Erin, W. Hu, M. Sitti, *Proc. Natl. Acad. Sci. USA* **2016**, *113*, E6007.
- [80] W. Hu, G. Z. Lum, M. Mastrangeli, M. Sitti, *Nature* **2018**, *554*, 81.
- [81] J. V. Timonen, C. Johans, K. Kontturi, A. Walther, O. Ikkala, R. H. Ras, *ACS Appl. Mater. Interfaces* **2010**, *2*, 2226.
- [82] a) R. M. Erb, J. J. Martin, R. Soheilian, C. Pan, J. R. Barber, *Adv. Funct. Mater.* **2016**, *26*, 3859; b) H. Lee, J. Kim, J. Kim, S. E. Chung, S.-E. Choi, S. Kwon, *Nat. Mater.* **2011**, *10*, 625.
- [83] Y. Kim, H. Yuk, R. Zhao, S. A. Chester, X. Zhao, *Nature* **2018**, *558*, 274.
- [84] T. Ikeda, J.-i. Mamiya, Y. Yu, *Angew. Chem., Int. Ed.* **2007**, *46*, 506.
- [85] M. Yamada, M. Kondo, R. Miyasato, Y. Naka, J. Mamiya, M. Kinoshita, A. Shishido, Y. L. Yu, C. J. Barrett, T. Ikeda, *J. Mater. Chem.* **2009**, *19*, 60.
- [86] J. Naciri, A. Srinivasan, H. Jeon, N. Nikolov, P. Keller, B. R. Ratna, *Macromolecules* **2003**, *36*, 8499.
- [87] M. Rogóż, H. Zeng, C. Xuan, D. S. Wiersma, P. Wasylczyk, *Adv. Opt. Mater.* **2016**, *4*, 1689.
- [88] S. Ahmed, E. Arrojado, N. Sigamani, Z. Ounaies, in *Behavior and Mechanics of Multifunctional Materials and Composites 2015* (Ed: N. C. Goulbourne), Vol. 9432, SPIE, Bellingham, WA **2015**, pp. 29–41.
- [89] Q. Chen, D. Natale, B. Neese, K. Ren, M. Lin, Q. Zhang, M. Pattom, K. Wang, H. Fang, E. Im, in *Electroactive Polymer Actuators and Devices (EAPAD) 2007* (Ed: Y. Bar-Cohen), Vol. 6524, SPIE, Bellingham, WA **2007**.
- [90] J. D. Carrico, K. J. Kim, K. K. Leang, in *2017 IEEE Int. Conf. on Robotics and Automation (ICRA)*, IEEE, Piscataway, NJ **2017**, pp. 4313–4320.
- [91] C. S. Haines, M. D. Lima, N. Li, G. M. Spinks, J. Foughri, J. D. Madden, S. H. Kim, S. Fang, M. J. De Andrade, F. Göktepe, *Science* **2014**, *343*, 868.
- [92] Y. Yang, Y. A. Tse, Y. Zhang, Z. Kan, M. Y. Wang, in *2019 2nd IEEE Int. Conf. on Soft Robotics (RoboSoft)*, IEEE, Piscataway, NJ **2019**, pp. 161–166.
- [93] X. Tang, K. Li, Y. Liu, D. Zhou, J. Zhao, *Sens. Actuators, A* **2019**, *291*, 80.